

# Sub-Scalp EEG for Sensorimotor Brain-Computer Interface

T B Mahoney<sup>1</sup>, D B Grayden<sup>1,2</sup>, S E John<sup>1</sup>

<sup>1</sup>Department of Biomedical Engineering, University of Melbourne, Victoria, 3010, Australia.

<sup>2</sup> Graeme Clark Institute, University of Melbourne, Victoria 3010, Australia.

E-mail: tmmah@unimelb.edu.au

## Abstract.

**Objective:** To establish sub-scalp electroencephalography (EEG) as a viable option for brain-computer interface (BCI) applications, particularly for chronic use, by demonstrating its effectiveness in recording and classifying sensorimotor neural activity.

**Approach:** Two experiments were conducted in this study. The first aim was to demonstrate the high spatial resolution of sub-scalp EEG through analysis of somatosensory evoked potentials in sheep models. The second focused on the practical application of sub-scalp EEG, classifying motor execution using data collected during a sheep behavioural experiment.

**Main Results:** We successfully demonstrated the recording of sensorimotor rhythms using sub-scalp EEG in sheep models. Important spatial, temporal, and spectral features of these signals were identified, and we were able to classify motor execution with above-chance performance. These results are comparable to previous work that investigated signal quality and motor execution classification using ECoG and endovascular arrays in sheep models.

**Significance:** These results suggest that sub-scalp EEG may provide signal quality that approaches that of more invasive neural recording methods such as ECoG and endovascular arrays, and support the use of sub-scalp EEG for chronic BCI applications.

**Index terms**— somatosensory evoked potential, motor execution, minimally invasive, spatial resolution, signal-to-noise ratio

## 1. Introduction

Tetraplegia, or paralysis of the arms and legs, can result from stroke, brain/spinal cord trauma, and a range of neurodegenerative disorders, which are becoming increasingly common with the ageing global population. [1, 2]. For individuals with these disabilities, communication, mobility, and general interaction with their environment can be difficult. Assistive devices, such as joysticks and eye-trackers, use residual muscle control to allow the user to interface with wheelchairs, robotic prostheses, and computers [3, 4]. Rather than rely on limited muscle control, brain-computer interfaces (BCIs) can detect neural activity from paralysed muscles and use it to control devices, offering greater freedom of movement [5, 6]. Despite the benefit these systems can provide, EEG BCIs are not used outside of research environments.

Surveys of potential BCI users have established that lengthy donning and doffing procedures, maintenance, instability, and aesthetics of EEG systems make for poor chronic in-home use [7–11]. Despite these pain points, users generally prefer non-invasive electrodes over implants [12]. Endovascular stent-electrode arrays offer a minimally invasive alternative signal acquisition method for BCIs [13]. However, currently endovascular BCIs cannot record activity from brain regions distal to large vasculature (namely the transverse and superior sagittal sinus), though ongoing research is focused on scaling stents to deploy in peripheral vessels [14, 15]. Situating electrodes such that they record from independent neural sources is important for BCI functionality, as the user’s modulation of these sources facilitates BCI control. Due to the poor spatial coverage of endovascular electrodes, current endovascular BCI are limited to a binary output, allowing the user to select output options when highlighted through an automated scrolling application or with eye-tracking-assisted selection. Additionally, the endovascular array cannot be removed post implantation in the event of failure, and carry risk of stenosis and thrombosis [16–18]. There is a need for an alternative method of chronic EEG recording for BCI applications.

Sub-scalp EEG is a recent innovation in the neural signal acquisition space that addresses many of the limitations of traditional surface EEG setups and endovascular arrays. Sub-scalp EEG has already demonstrated safety and stability from chronic implantation in persons with epilepsy, and sufficient signal quality for seizure monitoring [19–23]. Compared to external EEG caps, sub-scalp devices require no daily setup and are aesthetically discrete. Unlike endovascular arrays however, sub-scalp EEG can be removed and does not require access to critical

vasculature. Additionally, sub-scalp arrays offer the flexibility to be positioned across the skull as needed, thereby accessing neural signals from cortical regions distal to major vasculature. This broader spatial coverage is anticipated to enable sub-scalp EEG to facilitate higher-dimensional BCI inputs, moving beyond the binary systems currently employed with endovascular arrays. Examples include two-dimensional [24, 25] and three-dimensional cursor control [26] already demonstrated with non-invasive EEG, and may also extend to the rapidly developing field of speech decoding [27]. Previous studies have provided insights into sub-scalp EEG signal quality through comparison with alternative modalities. Sub-scalp EEG may record with similar signal quality, and thus BCI functionality, to non-invasive EEG, given the skull, rather than the scalp, is the major contributor of neural signal attenuation [28]. Generally, when compared to non-invasive EEG recordings, sub-scalp EEG has demonstrated: similar or higher signal quality and reduced artefacts due to line noise, eye movements, and electrode shift, but similar or increased electromyography artefact, which is likely due to the proximity to the temporalis muscle [19, 29–31]. Olson et al. [32] investigated similarities between sub-scalp EEG and ECoG, with a focus on signal bandwidth, demonstrating that sub-scalp EEG could record high-gamma activity up to 110 Hz, but with lower power than ECoG. Previous preliminary work has demonstrated comparable sub-scalp EEG signal amplitude, signal-to-noise ratio, and bandwidth to endovascular electrodes in sheep models [33]. However, spatial resolution of sub-scalp EEG recordings is unclear. High spatial resolution is one of the primary motivators for intracranial recording methods such as electrocorticography (ECoG) over non-invasive EEG [34–39]. Characterising the spatial resolution of sub-scalp EEG recordings will provide insight into what performance to expect from a sub-scalp BCI device.

Previous work has explored spatial resolution with current signal acquisition methods (Figure 1). Non-invasive EEG has typically demonstrated an optimal inter-electrode distance in the order of tens of millimetres [40–43]. Other work has investigated spatial resolutions of ECoG arrays [40, 44], reporting optimal distances as low as 1.25 mm [45]. More recent work has examined electrode size and spacing in novel endovascular electrode arrays and demonstrated equivalent spatial resolution with epidural and subdural ECoG [44]. While we hypothesise that sub-scalp EEG will have a spatial resolution between non-invasive EEG and intracranial electrodes (1 to 10 mm), the optimal inter-electrode distance is unknown.

This study comprises two aims toward investigating sub-scalp EEG feasibility

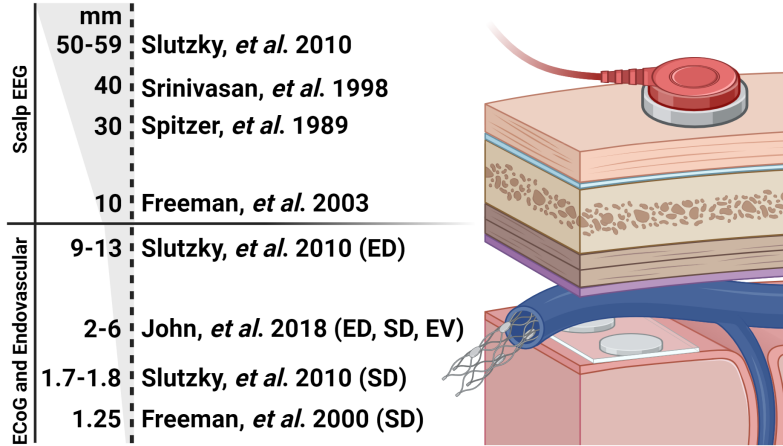


**Figure 1:** Outcomes of prior studies investigating optimal inter-electrode distances of neural recording methods: scalp EEG, ECoG (ED=epidural, SD=subdural), and endovascular (EV). (Created using biorender.com)

for sensorimotor BCI applications. These are:

Aim 1: Investigate the spatial resolution of sub-scalp EEG somatosensory evoked potentials (SEP).

Aim 2: Demonstrate sensorimotor activity decoding with sub-scalp EEG.

We performed *in vivo* recording of SEPs in sheep models. SEPs are evoked in the somatosensory cortex, in response to peripheral sensorimotor stimulus. In human models, the SEP waveform is often in the order of microvolts, and are generally localised to the posterior portion of the central sulcus [46]. Being within a sulcus, SEP phases change depending on the relative location of the recording electrode. With sufficient signal quality, these phase changes can be used to locate the somatosensory cortex [47]. The first aim of this study was to investigate the spatial resolution of sub-scalp EEG by examining spatial variations in SEP signal-to-noise ratio (SNR) and phase.

The second aim was to demonstrate decoding of sensorimotor activity recorded from sub-scalp EEG in animal models to provide supporting evidence toward sBCI feasibility. We analysed sub-scalp EEG recordings from sheep models during a forced-choice behavioural task, and successfully decoded motor execution. We compare our results with an identical study performed previously with data recorded from an endovascular array [48] and report strong similarity in performance. Our research



offers practical recommendations for the design of sBCI arrays, including guidelines for appropriate electrode size and spacing. Furthermore, the successful decoding of sensorimotor activity confirms the feasibility of using sub-scalp EEG for brain-computer interface applications. Of the two aims, the findings of Aim 1 represent a significant advancement in our understanding of spatial resolution for electrodes placed in the sub-scalp space. While Aim 2 provides an interesting comparison to previous work with endovascular arrays, its findings are not as broadly generalizable as Aim 1, and its interpretation requires careful consideration of the experimental limitations, as described in Section 4.3. As such, greater detail and analysis were provided for Aim 1.

## 2. Methods

Both aims were investigated with adult female sheep models. The research was approved by the Animal Ethics Committee of the Florey Institute of Neuroscience and Mental Health, Melbourne, Australia (Approval number: 22010), which operates in accordance with the Australian Code for the care and use of animals for scientific purposes (8th edition 2013). Acute SEP stimulation experiments were performed to collect data for Aim 1. Aim 2 used data collected from sheep during a forced choice behavioural task. All analyses were performed in MATLAB (Version 2023a, MathWorks, USA).

### 2.1. Acute SEP Experiment

The purpose of this experiment was to investigate the spatial resolution of sub-scalp EEG SEP recordings.

*2.1.1. Surgical Procedure* During both the array implantation and the stimulation procedures, the sheep were induced using an intravenous injection of sodium thiopentone, and anaesthesia was maintained with isoflurane (1–2.0% minimum alveolar concentration (MAC)). The sheep were euthanised at the conclusion of each experiment via pentobarbitone injection.

A 30 mm incision was made laterally across the scalp, posterior to the motor cortex. A spatula was used to separate the periosteum from the skull above the ovine sensorimotor cortex regions (as understood by previous research [49]) in an area

large enough to allow insertion of the electrode arrays over the skull (approximately  $30 \times 30$  mm). The arrays were placed laterally off centre by 10 mm, contralateral to the side of stimulation.

An incision was made in the forelimb midway between the elbow and knee joints. The electrode array used for stimulation (Figure 2a) was inserted beneath the skin and wrapped around the musculature. After applying stimulation to each electrode individually, the electrode that most readily produced muscle contraction was used for the experiment.

*2.1.2. Electrode Arrays* The size of electrodes can impact spatial resolution. Small electrodes, intracranial electrodes in particular, can record signals of interest from local regions with little noise from more distal regions [50]. As electrode size increases, the electrodes record activity from regions of the brain that are outside of the region of interest, thereby increasing the noise component of the recording, and reducing spatial resolution. To account for this, we compare responses between arrays with different electrode diameters.

The electrode arrays were custom designs, manufactured on a two-layer flex PCB (polyimide, 0.22 mm thickness) by PCBway (China). Three array designs were used. The large array was a  $3 \times 3$  grid with 10 mm inter-channel distance, or pitch, and 5 mm electrode diameter (Figure 2b). The medium array was a  $5 \times 5$  grid of electrodes with 5 mm pitch and 3 mm diameter (Figure 2c). The small array was also a  $5 \times 5$  grid with 5 mm, although with 1 mm electrode diameter (Figure 2d). In this paper, arrays will be referred to by their electrode diameter. The arrays included ground and reference electrodes on the back (facing the scalp). All electrodes were gold plated at manufacture. Recording was performed using the G.USBamp amplifier system (g.tec Medical Engineering, Austria), with a sampling frequency of 4800 Hz. The amplifier's high channel count and sampling frequency provided the necessary capabilities for this experiment.

*2.1.3. Stimulation Procedure* Stimulation was applied to the forelimb using a constant current stimulator (ISO Flex, A.M.P.I., Israel), controlled by a signal generator (Master 9, A.M.P.I., Israel). The stimulation threshold was determined by varying stimulation current between 0.5-10 mA in 0.5 mA intervals until muscle contraction was noticeable by eye. Stimulation was then applied to the forelimb with currents ranging between  $\pm 2$  mA of this threshold, at intervals of 0.5 mA. Stimulation

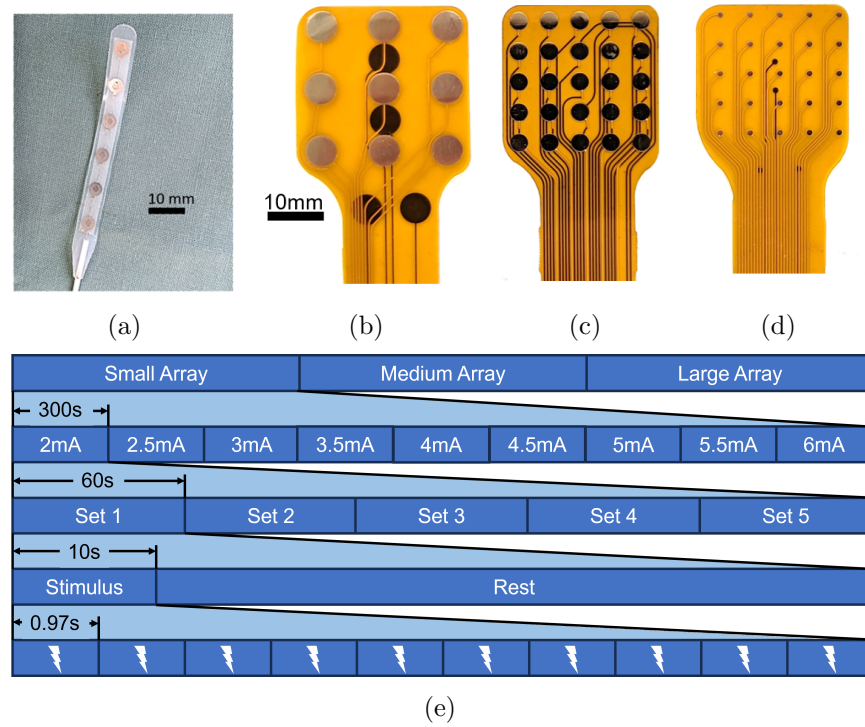


**Figure 2:** Electrode arrays and testing procedure. (a) The electrode array used for subcutaneous stimulation to the forelimb. The (b) large (5 mm), (c) medium (3 mm), and (d) small (1 mm) custom sub-scalp arrays. The reference and ground electrodes can be seen through the substrate on the back of the arrays. These figures are the same scale. (e) A breakdown of the stimulus experiment session. Stimulus pulses were applied once a second for ten seconds, followed by 50 s of rest. This was repeated five times per stimulus amplitude for nine amplitudes about the threshold. This figure illustrates the stimulus process, for example, for a threshold amplitude of 4 mA.

was applied in 1 min sets comprising ten 500  $\mu$ s stimuli separated by 997 ms, followed by 50 s of rest to mitigate risk of stimulus fatigue (Figure 2e). Stimulus current was increased after five sets resulting in 50 repetitions for each of the nine current levels. This process was repeated for the three array sizes. A trigger signal from the signal generator to the amplifier was used to annotate the exact time of stimulation.

*2.1.4. Data Preprocessing* The data were prepared for analysis using the following process:

- (i) Stimulus artefact removal: the stimulus creates a high amplitude artefact in the recorded data. Filtering the data without removing the stimulus artefact causes a ringing artefact that masks the stimulus response; thus, the stimulus must be removed before filtering. Due to power line noise, there is a prominent periodic signal occurring at 50 Hz. Simple linear interpolation or splining across the stimulus artefact disrupts this dominant frequency, which also leads to ringing artefact when filtering. To remove the artefact, 32 samples post-trigger were replaced with the 32 samples that occurred 96 samples prior (20 ms or one 50 Hz period).
- (ii) Filtering: The data was filtered with a series of 20th order, zero-phase IIR filters. These included notch filters at 50, 100, and 150 Hz to remove power line noise, and a bandpass filter between 10 and 190 Hz.
- (iii) Trial rejection: The data was split into epochs spanning 70 ms before and after each stimulus. Trials with a sample standard deviation greater than the 80th percentile were considered too noisy and were rejected.
- (iv) Re-referencing: Trials were re-referenced using common average referencing (CAR).
- (v) Channel rejection: Channels were rejected by eye through observation of the average-over-trial epochs.
- (vi) Current threshold: The stimulus current threshold was determined as that which produced a response visually. The lowest stimulus current that resulted in a noticeable response in the average-over-trials EEG epochs for each experiment was used for analysis.

*2.1.5. Signal-to-Noise Ratio (SNR)* SNR was computed for each trial as the ratio of the variance of the data from 10-70 ms after the stimulus to the variance of the data 10-70 ms prior to the stimulus. To ensure high-quality recordings, an array should exhibit high SNR on channels near the neural activity and low SNR on distal channels. Thus, high SNR was not expected on all channels. To assess the array's capacity to record high SNR signals, the two channels with the highest SNR across experiments were compared.

*2.1.6. Cross-correlation* Cross-correlation was used to identify common SEP spatial activity and the lag between different electrodes. Pairwise cross-correlation was

calculated for average-over-trials SEPs, between channels that recorded with median SNR  $> 0$  dB and was scaled such that autocorrelations with zero lag equal to one. Maximum correlations within a  $\pm 5$  ms lag are reported.

## 2.2. Behavioural Experiment

The behavioural experiment to test Aim 2 closely followed previous work examining motor-related neural activity recorded with endovascular stent-electrode arrays by Forsyth et al. [48].

*2.2.1. Electrode Array* For Aim 1, cost-effective custom thin-film arrays were employed due to their configurable nature and suitability for acute experimental conditions. In contrast, Aim 2 necessitated an array optimised for chronic implantation, leading to the selection of a commercially available array designed for clinical neural recording. The electrode array (AirRay, Cortec, Germany) was a 32-channel ( $4 \times 8$ ) grid array, measuring  $20 \times 20$  mm, with platinum electrodes ( $\varnothing$  1 mm). The array was embedded in firm silicone (M4670, Barnes Products Pty Ltd, Australia) to provide anchorage points (Figure 3a). The cabling was encased within flexible tubing that was flooded with silicone (Permatex Canada Inc., Canada) to reduce the risk of interstitial fluid ingress.

*2.2.2. Implantation Procedure* The sub-scalp array was implanted in four female corriedale sheep. The sheep were anaesthetised during implantation with isoflurane. Two 60 mm wide incisions were made laterally across the scalp down to the skull, one anterior and one posterior to the motor cortex. The array was sterilised in an ethanol bath prior to implantation. The electrode array was inserted into the cavity, directly onto the skull surface. The array was sutured into place. The cabling was tunnelled from the scalp site down to the shoulder where it exited the skin through a small incision. The incision sites were then sutured closed. Behavioural experiments began one week after implantation. The device remained *in vivo* for three weeks post implantation. Figure 3b is an x-ray image of an animal prior to array removal, showing the placement over the motor cortex as understood by previous ovine studies [49, 51].

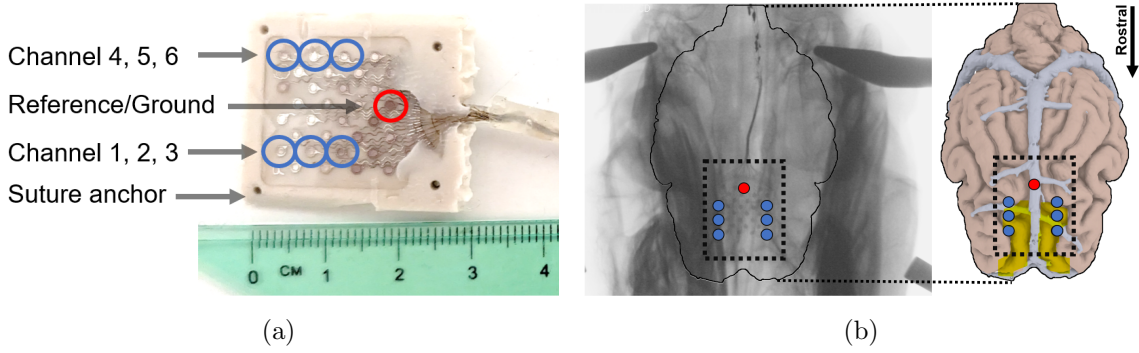


**Figure 3:** Electrode array and location. (a) The electrode array (AirRay, Cortec, Germany) encased in silicone (M4670, Barnes Products Pty Ltd, Australia) with anchorage points for suturing at each corner. The wires were encased within an intravenous tubing set flooded with silicone (Permatex Canada Inc., Canada). Channels are indicated by the blue circles and reference/ground by the red circle. (b) An x-ray image of the sheep head with the array (outlined by the black, dashed rectangle) implanted above the motor cortex, as indicated by the adjacent sheep brain model (source: Oxley et al. [52]).

*2.2.3. Amplifier* Unlike Aim 1, this experiment necessitated an amplifier with a lower channel count and a portable design. Portability was crucial to reduce cable length and prevent motion artifacts, ensuring the animal’s unrestricted movement. As such, the amplification hardware used for the behavioural experiment was a portable module worn on the animal, comprising an Intan RHD2032 chip (Intan Technologies, USA) that sampled six channels with 1024 Hz sampling frequency per channel.

*2.2.4. Behavioural Experiment Setup* The behavioural experimental setup was similar to a previous experiment performed by Forsyth et al. [48], and is illustrated in Figure 4. The animals were housed in individual cages. In front of each animal were three touch buttons with light emitting diodes (LEDs). The buttons were positioned at head height, within reach of the head. One button was directly in front of the animal, one was to the left, and the other was to the right. Also, in front of the animal were two audio speakers, a food trough within reach of the animal, and a camera facing the animal.

The behavioural task was used to encourage the animal to perform left and right head movements. The animal was taught the task in a series of stages as follows:

- (i) The equipment was set up around the animal. Food was provided in rations frequently until the animal appeared at ease with the setup and the experimenter.
- (ii) The centre button was lit up. When the animal touched the button, a single high pitched correct tone was sounded and the animal was fed a ration immediately. This continued until the animal appeared to understand the task.
- (iii) The centre button was lit up. Upon touching the centre button, one of either the left or the right buttons was lit up at random. If the animal touched the lit button within 20 seconds, a high-pitched correct tone was sounded and the animal was fed immediately. If the animal did not touch the button within the time limit, a lower pitched incorrect tone was sounded and a delay of 20 seconds prevented the animal from starting another trial. EEG data collection was started once the animal appeared to understand the task.

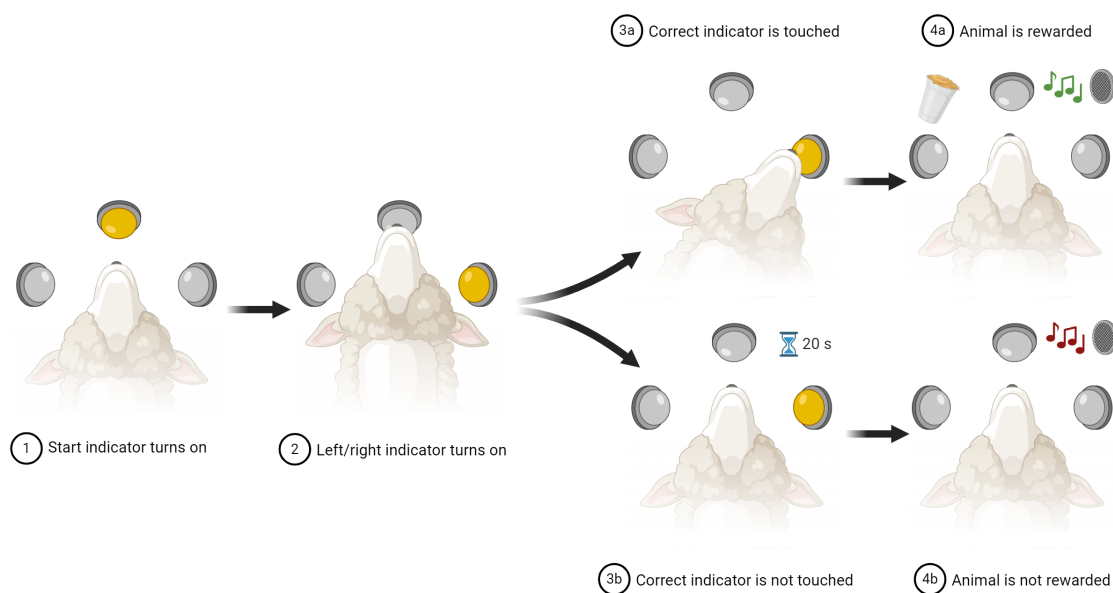


**Figure 4:** The behavioural experiment progression during a single trial where the animal either successfully completes the task and is presented with a tone indicating success and a reward (3a and 4a), or fails (3b and 4b) and receives a tone indicating failure and no reward (created with BioRender.com).

The feed ration was 125 ml of a 50/50 mix of chaff/lucerne. Trials continued

until either the animal lost interest or their daily allotment of food was consumed. In all cases where the animal lost interest in the task, they were fed the remainder of their daily allotment of food.

A Python script received serial triggers when the left or right buttons were pressed, as well as Bluetooth EEG data from the Intan amplifier. The camera captured the moment the animal began head movement in the direction of the button. The video combined with the timing information allowed investigation of the sub-scalp EEG during and prior to motor activity.

*2.2.5. Analysis Procedures* The data were bandpass filtered between 2-200 Hz and re-referenced to a common average reference. The video footage was used to determine the time that head movement began toward the target, and the data were separated into epochs spanning 200 ms prior to movement and 500 ms post movement. Spectrograms of the epochs were created using the continuous wavelet transform (MATLAB's `cwt` function). In chronological order, every fifth epoch (20%) was set aside as a test set.

A filter feature selection algorithm was implemented to reduce the risk of overfitting. Features were selected by evaluating the mutual information between the labels of each trial and the feature set, spanning temporal, spectral, and spatial dimensions. The temporal feature set was restricted to 100 ms windows (no overlap) spanning the 200 ms before and the 500 ms after movement onset.

The frequency space comprised the bands theta [5-8 Hz], alpha [8-12 Hz], beta [12-30 Hz], gamma [30-70 Hz], and high gamma [70-200 Hz]. With the inclusion of six channels, the feature set included a total of 210 features.

Mutual information was computed by discretising the power measures using k-nearest neighbours [53] with publicly available MATLAB code [54]. The 15 features with the highest mutual information were chosen for classification.

Classification was performed using linear discriminant analysis. We evaluated both 2-class (left vs. right) and 3-class (left vs. right vs. rest) classification cases. Rest epochs were extracted from the data by sampling random EEG sections that did not overlap with movement epochs. Feature selection and classification was performed within a five-fold cross validation (CV) rotation. We also report the classification result of the unseen test set having trained a final model on the entire training set. We used animal-specific feature selection and classification models to overcome inter-animal variation in feature importance. A binomial test was used to



determine if classification was above chance.

### 3. Results

#### 3.1. SEP Stimulation Results

For Aim 1, the experiment was performed on eight forelimbs for the 1 mm array, and seven forelimbs for the 3 mm and 5 mm arrays, across four sheep (see table 1). Each forelimb experiment will be referred to as a session, session 1 being sheep 1, with stimulation to the left forelimb. 37%, 22%, and 29% of channels for the 1 mm, 3 mm, and 5 mm arrays, respectively, were rejected by eye.

Figures 5a, 5b, and 5c display exemplary single-trial SEP recordings from the 1 mm, 3 mm, and 5 mm arrays, respectively. The bold line indicates the average-over-trials SEP. In the 1 mm and 3 mm arrays, the SEP appears as a positive potential approximately 25 ms post stimulus (indicated by the dashed line), followed by a negative potential at approximately 50 ms post stimulus. SEP waveforms varied, as depicted in Figure 5d, which displays the approximate placement of the array over the ovine sensory and motor cortices and examples of recorded averaged-over-trials SEP responses from the 1 mm, 3 mm, and 5 mm arrays. As illustrated in the traces displayed in the figure, we typically observed variations in phase and amplitude of the SEP responses across electrodes in recordings from 1 mm and 3 mm size electrodes, though not 5 mm electrodes. While previous work has noted both contralateral and ipsilateral SEP responses in sheep models [49], there was no obvious laterally reflected spatial patterns observed between stimulus applied to the left forelimb versus the right forelimb.

Figure 5d also illustrates the spatial variation in SNR and inter-channel correlation. Within these maps, there are channels that recorded SEPs with distinct variation in SNR and correlation to adjacent channels. For example, concerning the 3 mm array, channel 19 recorded SEPs with relatively low SNR compared to adjacent channels 13, 14, 15, 20, and 24, although with similar SNR to channel 18. SNR and correlation results are discussed further in Sections 3.1.1 and 3.1.2, respectively. For all average-over-trials traces, and SNR and correlations maps, refer to Supplementary Materials.

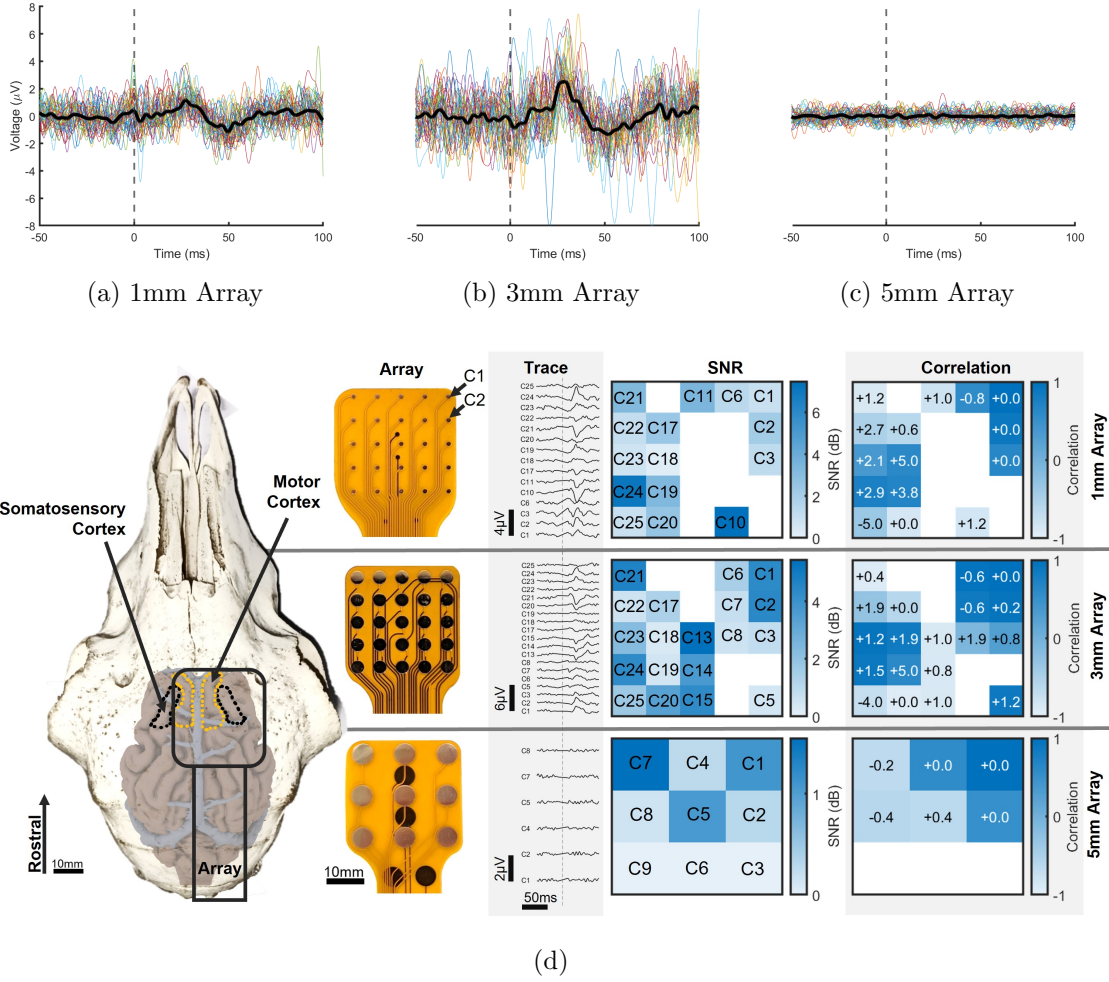


**Figure 5:** SEP Responses. Exemplar single trial SEP recordings from the (a) 1 mm, (b) 3 mm, and (c) 5 mm arrays in the same animal. The average over trials is shown in bold. The dashed line indicates the time of stimulus. These figures share the same voltage scale. (d) Examples of the array placement location over the the sheep skull and approximate location of the motor and somatosensory cortices beneath, as according to John et al. [49]. For each array are shown exemplary average-over-trial traces, an SNR heatmap, and a correlation heatmap across channels. For the SNR heatmap, the text indicates the corresponding channel and the colour indicates the SNR amplitude. For the cross-correlation heatmap, the colour indicates the peak correlation within a  $\pm 5$  ms delay of channel 1, and the text indicates the correlation peak delay in milliseconds. White heatmap segments indicate either the rejection of a channel due to noise, or  $\text{SNR} < 0$  dB. This data was all collected from the same session (S5).

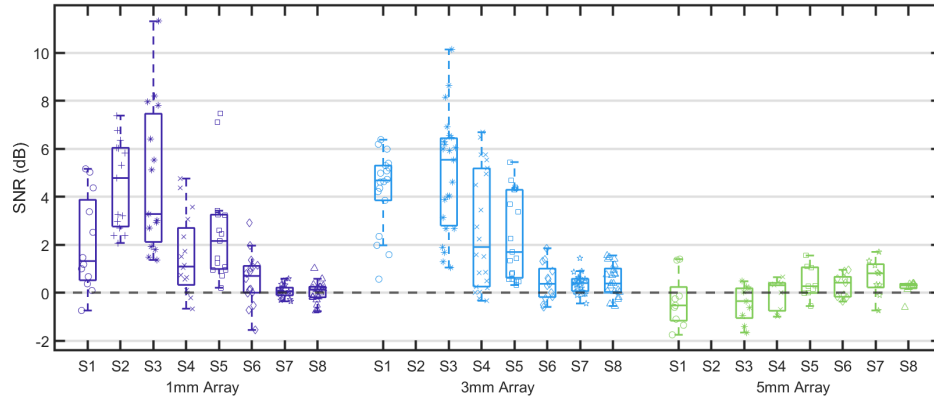
**Table 1:** Recording sessions (S1 to S8) across the stimulation of left (L) and right (R) forelimbs of each of the four sheep. The symbols are used to indicate sessions in subsequent figures. There were no 3 mm or 5 mm array recordings for S2 due to time constraints.

|            | Sheep |    |    |    |    |    |    |    |
|------------|-------|----|----|----|----|----|----|----|
|            | 1     |    | 2  |    | 3  |    | 4  |    |
|            | L     | R  | L  | R  | L  | R  | L  | R  |
|            | S1    | S2 | S3 | S4 | S5 | S6 | S7 | S8 |
| Array Size |       |    |    |    |    |    |    |    |
| 1 mm Array | ○     | +  | *  | ×  | □  | ◇  | ☆  | △  |
| 3 mm Array | ○     |    | *  | ×  | □  | ◇  | ☆  | △  |
| 5 mm Array | ○     |    | *  | ×  | □  | ◇  | ☆  | △  |

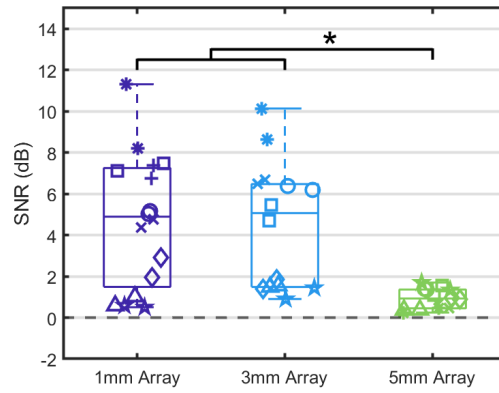
*3.1.1. Signal-to-Noise Ratio (SNR)* Figure 6a shows the spread of SNR across channels for each array and session. The median SNR across channels was significantly greater than 0 dB in 5 of the 8 sessions (62.5%) with the 1 mm array, 6 of the 7 sessions (85.7%) with the 3 mm array, and 0 of the 7 sessions (0%) with the 5 mm array ( $\alpha = 0.01$ , Student's t-test). P-values for each session are provided in table 2. SNR varied more between channels in sessions recorded with the 1 mm array ( $\sigma^2=3.1\pm3.0 \mu V^2$ , median $\pm$ std across sessions) and 3 mm array ( $\sigma^2=2.7\pm2.6 \mu V^2$ ) recordings compared to the 5 mm array ( $\sigma^2=0.4\pm0.35 \mu V^2$ ).

Figure 6b is a comparison of the two channels with the highest SNR for each session, across array types. One-way ANOVA revealed a significant difference between the groups,  $F(2, 41) = 9.48$ ,  $p=0.0004$ . Post-hoc analysis (Tukey's HSD) indicated that the top-two SEP SNRs recorded from 1 mm and 3 mm electrodes were significantly greater than those recorded using 5 mm electrodes ( $p=0.0006$  and  $p=0.0017$ , respectively,  $\alpha = 0.01$ ). There was no significant difference between SNR from 1 mm and 3 mm electrodes ( $p=0.9659$ ). All groups in Figure 6b recorded SEP SNR significantly greater than 0 db ( $p< 0.0001$ ,  $\alpha = 0.01$ , Student's t-test).

*3.1.2. Cross-Correlation* Cross-correlation varied across channels in each session and array. There were groups of adjacent channels with high positive correlation and groups of adjacent channels with high negative correlation. Figure 7a depicts the change in phase across channels from session 2, as recorded with the 1 mm



(a)



(b)

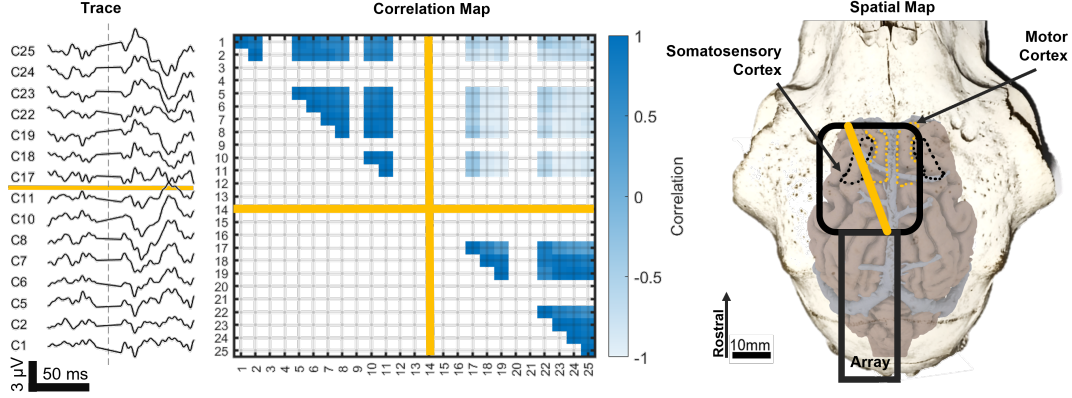
**Figure 6:** (a) The median SEP SNR for each channel across sessions and arrays. Each marker is the median SEP SNR across trials for a single channel. S1 to S8 are the different sessions. (b) The two channels with highest SNR grouped across sessions for each array. Each marker type indicates the recording session. The significance marker (\*) indicates a p-value less than 0.01.

array. This example has been highlighted as the phase change depicted two clearly separable groups, as illustrated by the orange line. In this example, channels 1 to 11 are correlated, forming a group on the correlation map. Although there is variation between these channels, generally they depict an SEP with a negative potential followed by a positive potential. Channels 17 to 25 are also positively

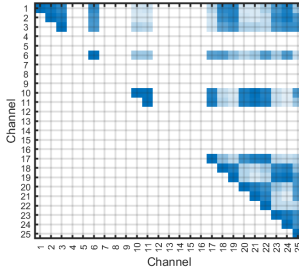
**Table 2:** The Student’s t-test p-values for each array and session to test if SNR is significantly greater than zero across all channels. We also include the percentage of sessions that recorded with SNR significantly greater than zero.

| Session        | Array      |            |            |            |        |            |
|----------------|------------|------------|------------|------------|--------|------------|
|                | 1 mm       |            | 3 mm       |            | 5 mm   |            |
|                | p          | $< \alpha$ | p          | $< \alpha$ | p      | $< \alpha$ |
| S1             | 0.0048     | true       | $< 0.0001$ | true       | 0.3958 | false      |
| S2             | $< 0.0001$ | true       |            |            |        |            |
| S3             | $< 0.0001$ | true       | $< 0.0001$ | true       | 0.1136 | false      |
| S4             | 0.0020     | true       | 0.001      | true       | 0.8236 | false      |
| S5             | 0.0005     | true       | $< 0.0001$ | true       | 0.0910 | false      |
| S6             | 0.0481     | false      | 0.0536     | false      | 0.1182 | false      |
| S7             | 0.4011     | false      | 0.0004     | true       | 0.0363 | false      |
| S8             | 0.7796     | false      | 0.0017     | true       | 0.2304 | false      |
| % p $< \alpha$ | 62.5%      |            | 85.7%      |            | 0.0%   |            |

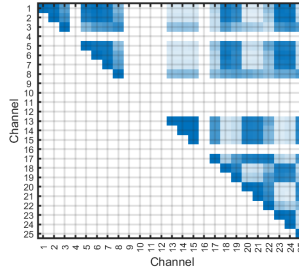
correlated, and are negatively correlated to channels 1 to 11. This relationship can be observed in the traces, where the SEP of these channels is instead a positive potential followed by a negative potential. Typically, as depicted in Figures 7b to 7d and further in Supplementary Materials, correlations were clustered in smaller, disconnected groups.



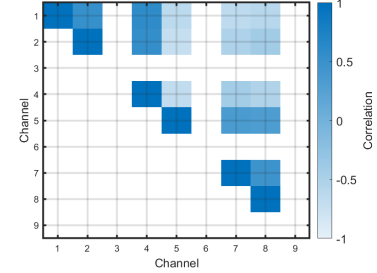
(a) S2, 1 mm Array



(b) S5, 1 mm Array



(c) S5, 3 mm Array



(d) S5, 5 mm Array

**Figure 7:** Pairwise channel correlation maps and histograms. (a) Phase variation across channels from one session (S2, 1 mm array). The traces on the left are the average-over-trial SEPs. The dashed line indicates the time of stimulus. The orange line illustrates the change in SEP phase between channels 1 to 11 and 17 to 25. This change in phase is consistent with computed inter-channel correlation values as per the adjacent heatmap, which depicts the pairwise channel correlations as a top-diagonal matrix. The map confirms that channels 1 to 11 and 17 to 25 form two groups comprising highly correlated channels, and that the groups are negatively correlated with each other. Similarly to the trace figure, the orange line between channels 11 and 17 discriminates between the two groups. On the right, the orange line is indicated spatial on the array, which is overlaid in the approximate location of recording. SEP (b), (c), (d) Examples of other correlation maps for each array from a single session (S5). White segments indicate either rejected channels or channels with SNR less than 0 dB.

### 3.2. Behavioural Results

For Aim 2, arrays were implanted in four sheep. All four animals successfully learned the task. At least 240 trials (120 left, 120 right) were recorded from each sheep across multiple sessions. Recording examples from sheep 1 are shown in Figure 8.

Figures 8a and 8b are the averaged-over-epochs EEG traces from sheep 1, depicting motor event related potentials. The potentials showed variations in amplitude and phase between left and right movements.

The frequency space revealed additional distinctions between left and right movements. Figures 8c and 8d are the mean spectrograms over all trials from sheep 1, channel 5, for left and right movements, respectively. As indicated by the dashed rectangle, there was a clear increase in power (synchronisation) across the theta, alpha, and beta frequency bands during left movement onset (Figure 8c) that was not recorded during right movement onset (Figure 8d). A comparison of the mean power spanning 0 to 100 ms post movement onset between left (blue) and right (yellow) movements is illustrated in Figure 8e. These findings demonstrate that useful features for movement classification were spread across different time windows, frequency bands, and channels.

### 3.3. Classification

Table 3 shows the classification results for both the 5-fold CV and test set models, as well as the number of trials tested on ( $n$ ), the resulting p-value, and the sensitivity and specificity for each class. For the two-class case of left vs. right movement classification, above chance performance ( $p < 0.05$ ) was achieved in two of the four animals, both in five-fold CV and the test set. Despite performing above chance in the test set ( $p = 0.032$ ), Sheep 2 classification accuracy was not considered above chance given the poor CV performance ( $p = 0.436$ ). When temporal features were limited to those prior to movement, performance was not above chance for any animals.

Considering the three-class case of left vs. right vs. rest classification, above chance performance was achieved in three of the four sheep in both CV and test sets. Data collected from sheep 4 failed to perform above chance level in any case.

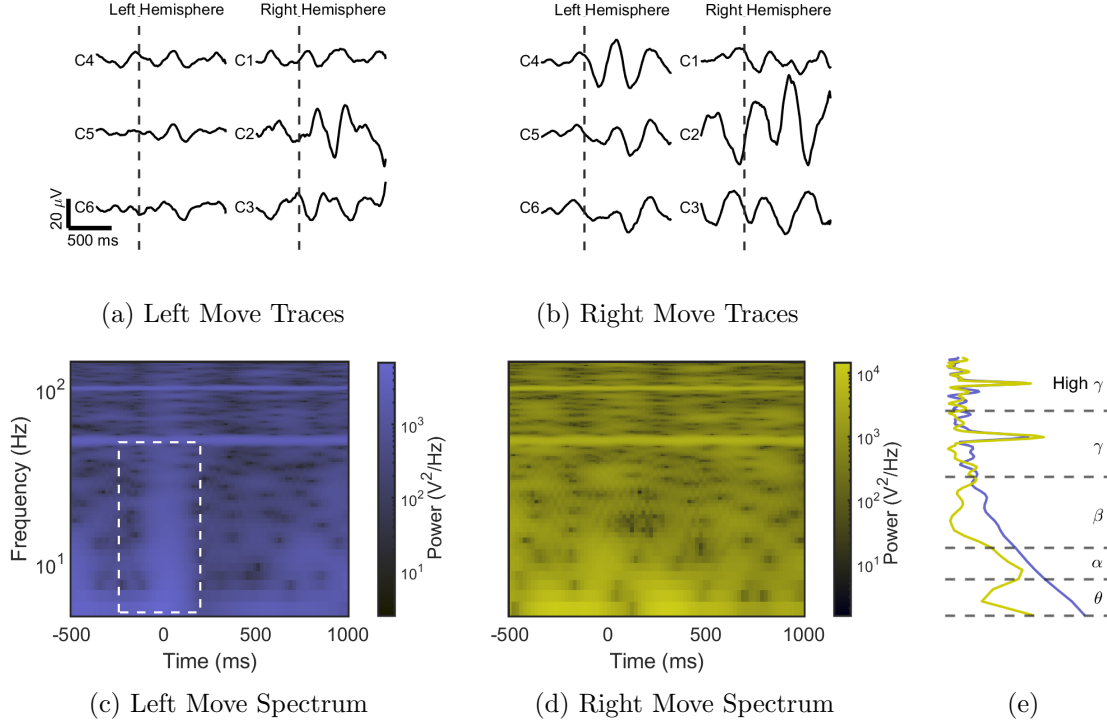


**Figure 8:** The averaged-over-trials traces for (a) left and (b) right movements in sheep 1. These traces were lowpass filtered with a cutoff of 30 Hz to help visualise the event related potentials. The dashed lines indicate the time of movement onset. The averaged-over-trials spectrograms of the (c) left and (d) right movement of sheep 1, as recorded by channel 5 (C5). The time scale is relative to movement onset. (e) The mean log-power spectra during the 0-100 ms window post stimulus. The line colour indicates the corresponding spectrum (blue - left movement, yellow - right movement). EEG frequency bands are indicated by the dashed lines.

Figure 9 shows the confusion matrices for each classification case test set, with cases resulting in above chance classification highlighted. Sheep 1 and 3 performed above chance in the two-class case, with sensitivity and specificity of 89% and 44%, and 68% and 65% respectively (left=positive, right=negative). For the three-class cases, the rest state had high mean class sensitivity for the motor execution case (74%) compared to the left and right classes (47% and 61%, respectively).



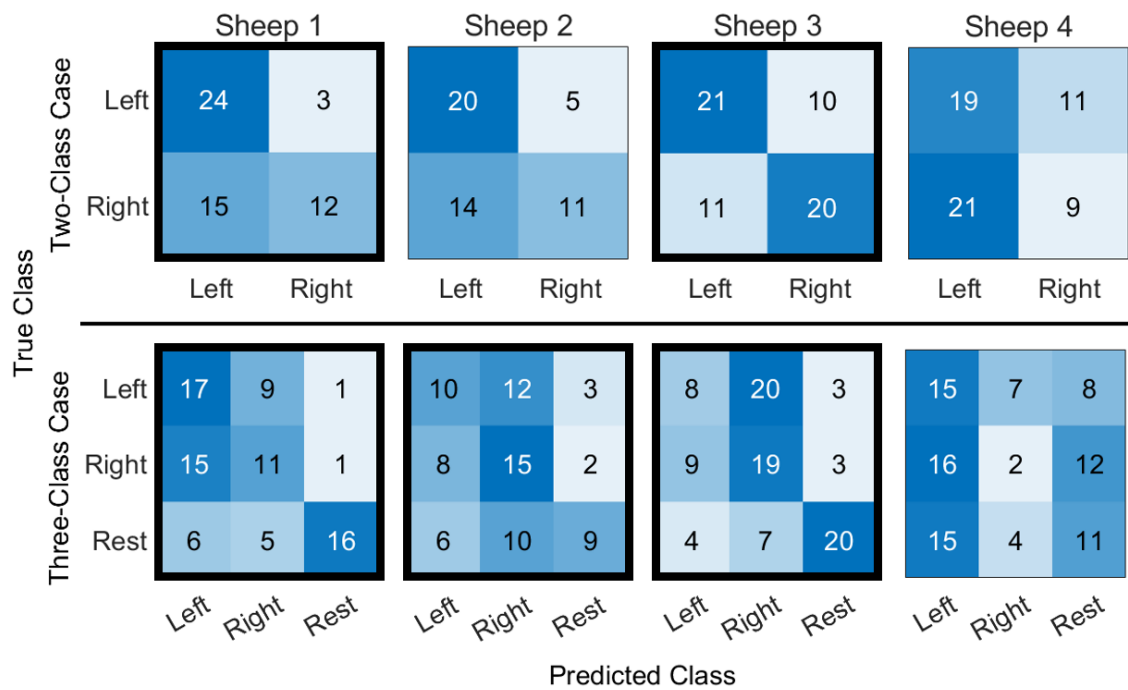


**Figure 9:** Confusion matrices for each classification case. The matrices with a bold outline indicate cases that resulted in above chance classification accuracy.

**Table 3:** Classification accuracy results of five-fold CV (mean $\pm$ std) and test set prediction for the two-class (left vs. right) and three-class (left vs. right vs. rest) cases. For each case, p-values and test set sizes ( $n$ ) are listed. Accuracy results in bold are significantly above chance ( $p < 0.05$ ). Classes were equally frequent in both training and test sets; hence chance level is 50% for the two-class case, and 33.3% for the three-class case.

| Left vs. Right          |                         |                             |         |    |                       |                |                            |                |                            |           |         |
|-------------------------|-------------------------|-----------------------------|---------|----|-----------------------|----------------|----------------------------|----------------|----------------------------|-----------|---------|
| Sheep                   | 5-Fold Cross Validation |                             |         |    | Test Set              |                |                            |                |                            |           |         |
|                         | n                       | Accuracy                    |         | n  | Class                 | Sensitivity    |                            | Specificity    |                            | Accuracy  |         |
|                         |                         | %                           | p-value |    |                       | %              | p-value                    | %              | p-value                    | %         | p-value |
| 1                       | 42                      | <b>65<math>\pm</math>15</b> | 0.021   | 54 | Left<br>Right         | 89<br>44       | <0.001<br>0.752            | 44<br>89       | 0.752<br><0.001            | <b>66</b> | 0.005   |
| 2                       | 38                      | 51 $\pm$ 8                  | 0.436   | 50 | Left<br>Right         | 80<br>44       | <0.001<br>0.760            | 44<br>80       | 0.760<br><0.001            | <b>62</b> | 0.032   |
| 3                       | 48                      | <b>67<math>\pm</math>9</b>  | 0.007   | 62 | Left<br>Right         | 68<br>65       | 0.002<br>0.008             | 65<br>68       | 0.008<br>0.002             | <b>66</b> | 0.004   |
| 4                       | 46                      | 56 $\pm$ 2                  | 0.231   | 60 | Left<br>Right         | 63<br>30       | 0.014<br>0.999             | 30<br>63       | 0.999<br>0.014             | 47        | 0.651   |
| Left vs. Right vs. Rest |                         |                             |         |    |                       |                |                            |                |                            |           |         |
| Sheep                   | 5-Fold Cross Validation |                             |         |    | Test Set              |                |                            |                |                            |           |         |
|                         | n                       | Accuracy                    |         | n  | Class                 | Sensitivity    |                            | Specificity    |                            | Accuracy  |         |
|                         |                         | %                           | p-value |    |                       | %              | p-value                    | %              | p-value                    | %         | p-value |
| 1                       | 63                      | <b>57<math>\pm</math>10</b> | <0.001  | 81 | Left<br>Right<br>Rest | 85<br>33<br>41 | <0.001<br>0.448<br>0.065   | 37<br>63<br>59 | 0.204<br><0.001<br><0.001  | <b>53</b> | <0.001  |
| 2                       | 57                      | <b>46<math>\pm</math>7</b>  | 0.019   | 75 | Left<br>Right<br>Rest | 52<br>44<br>68 | <0.001<br>0.020<br><0.001  | 56<br>60<br>48 | <0.001<br><0.001<br>0.003  | <b>55</b> | <0.001  |
| 3                       | 72                      | <b>52<math>\pm</math>13</b> | <0.001  | 93 | Left<br>Right<br>Rest | 61<br>58<br>68 | <0.001<br><0.001<br><0.001 | 63<br>65<br>60 | <0.001<br><0.001<br><0.001 | <b>62</b> | <0.001  |
| 4                       | 69                      | 36 $\pm$ 6                  | 0.347   | 90 | Left<br>Right<br>Rest | 67<br>10<br>23 | <0.001<br>1.000<br>0.974   | 17<br>45<br>38 | 1.000<br>0.011<br>0.157    | 33        | 0.540   |

## 4. Discussion

### 4.1. Aim 1: Sub-scalp EEG Spatial Resolution

Understanding the spatial resolution of EEG recorded from the sub-scalp space can provide supporting evidence for ventures seeking to develop sBCI systems for use with patients. The first aim of this study was to investigate the spatial resolution of sub-scalp EEG. We successfully recorded and analysed SEP responses from the sub-scalp space in animals models with arrays of varying electrode size. The results provide insight through analysis of spatial variations in SNR and correlation across channels. Our findings indicate that a 5 mm inter-channel distance reveals distinct spatial information, and that arrays with 1 mm and 3 mm electrode diameter record SEPs with higher SNR and inter-channel variance than arrays with 5 mm electrode diameter. Here, we will discuss the variations in SNR and correlation and relate them to spatial resolution, compare with alternative BCI signal acquisition methods, and note limitations of the work.

*4.1.1. Signal-to-Noise Ratio* The 1 mm and 3 mm diameter electrodes recorded SEPs with significantly higher SNR ( $4.9 \pm 3.2$  dB and  $5.1 \pm 3$  dB (median $\pm$ std), respectively) than the 5 mm electrodes ( $0.9 \pm 0.5$  dB). Larger electrodes record activity from broader areas. The 5 mm electrodes may have captured signals from such a large cortical area that their sensitivity regions overlapped, resulting in low SNR after common average referencing. While increasing the inter-channel distance may record less correlated signals, this would come at the cost of reduced spatial resolution.

The SNR values are in a similar range to previous work by John et al. [44], who also investigated SEP response in sheep, reporting single trial SNR from ECoG (epidural:  $\sim 5$  dB, subdural:  $\sim 8$  dB) and endovascular ( $\sim 5$  dB) arrays. Visual evoked potentials in sheep models have been recorded from endovascular arrays with similar single trial SNRs of 4.35 [55] and 4.77 dB (reported as  $3.05 \text{ V}^2/\text{V}^2$ ) [33]. However, direct comparison with these results is limited due to variations in the method of stimulation, hardware, data processing, and SNR calculation. Additionally, John et al. [44] allowed the electrodes to settle in the body for 3-4 weeks prior to recording, which would likely improve electrode contact and recording quality. Despite these differences in methods, recording SEP SNR with comparably high SNR to more

invasive ECoG and endovascular arrays suggests sub-scalp arrays may record with similarly high signal quality.

SNR also showed higher variance between channels with the 1 mm and 5 mm arrays ( $3.1 \pm 3.0 \mu V^2$  and  $2.7 \pm 2.6 \mu V^2$ , respectively) than the 5 mm arrays ( $0.4 \pm 0.3 \mu V^2$ ). High variance may indicate that spatial resolution is high enough to isolate neural regions where activity is comparatively low, such as regions distal to the somatosensory cortex. Additionally, low SNR may result from electrodes being positioned directly above a sulcus, where the electrode may not detect the electric fields generated by pyramidal neurons due to their orientation. In either case, SNR variance between channels suggests the 1 mm and 3 mm electrodes record with spatial resolution high enough to discriminate between activity from neural populations in close proximity.

*4.1.2. Correlation* The channels appear to form distinct functional groups. Channels within each group are highly correlated. Conversely, channels from different groups exhibit strong negative correlations, indicating that they may be recording activity from the same source, but with an opposing polarity. Previous work has demonstrated that variation in phase can relate to the electrodes location relative to the SEP, particularly when the source is located in a sulcus [46, 47]. This is commonly seen in intracranial electrodes, such as ECoG [56], but has also been demonstrated non-invasively with ultra high density EEG [47]. Most channels were either highly positively or negatively correlated. The observed differences in inter-channel correlation, and SNR, across channels are likely attributable to variations in the underlying brain anatomy, including sulcal and gyral patterns, skull thickness, and vasculature. These findings indicate that the sub-scalp EEG recordings have sufficient spatial resolution to differentiate neural activity originating from these various structures. However, the precise location of such structures relative to the arrays was not verified.

*4.1.3. Spatial Resolution* Spatial resolution increased when using higher density arrays. 1 mm and 3 mm diameter electrodes with 5 mm pitch recorded activity with distinct variations in SNR and correlation between adjacent channels. Together, these results suggests 5 mm inter-channel distance is not spatially oversampling. Current sub-scalp EEG devices have been developed for chronic seizure monitoring or detection of hypoglycaemia [20, 23], typically featuring less than 8 channels and

low sampling rates (250 Hz). Our findings indicate that higher density sub-scalp electrode arrays may have utility for brain-computer interface applications. Future work should aim to identify the minimum inter-channel distance for electrodes in the sub-scalp space through use of higher density arrays.

#### *4.2. Aim 2: Sub-scalp EEG Motor Decoding*

The behavioural experiment results suggest that sub-scalp EEG is suitable for BCI applications that utilise motor-related neural activity. We discriminated between left and right movement execution in two of four sheep, and movement in either the left or right direction vs. rest in three of four sheep. The results are comparable to similar work previously performed to test efficacy of endovascular electrode arrays for BCI applications [48]. Additionally, feature selection provided valuable insight into the importance of different temporal, spectral, and spatial qualities of sub-scalp EEG recordings.

*4.2.1. Feature Importance* The features that were most important for movement classification were different across the animals, demonstrating the importance of animal (or human) specific models for feature selection and classification. Regarding the frequency space, high gamma features most often demonstrated high mutual information with the class labels. High gamma is a useful feature for BCI applications as it has been shown to have more functional localisation than lower frequency bands, although it is difficult to detect with non-invasive EEG due to low amplitudes [57, 58]. This is the first demonstration of detection of high gamma features associated with motor function with sub-scalp EEG. This result supports sub-scalp EEG use in BCI applications and warrants further investigation as part of an online BCI system.

In contrast with prior understanding of sensorimotor activity in humans [59], the beta band was of minimal importance, being the least selected band across all sheep and classification cases. This may be due to physiological differences between human and sheep models, or it is possible that the availability of high-quality gamma and high gamma features may have taken precedence during feature selection.

Spatially, we observed some variation between the median spectrograms of each channel (Figure 8e). Typically in human models, there is a strong contralateral relationship between power modulation in the motor cortex and movement that aids in discriminating between motor activity from the left or right side of the body [59].

In sheep models, the motor cortices of both hemispheres are proximal to each other and extend along the rostral-caudal axis. As such, potentials measured by electrodes outside the skull will likely contain a summation of activity from sources across both hemispheres. This physiology may explain the poor sensitivity and specificity of the left and right classes as spatial features are critical for this discrimination. Recording neural activity with high resolution is beneficial for BCI applications as discriminating between activity in proximal brain regions can facilitate higher degrees of freedom. We expect brain structure to present fewer challenges in humans than sheep models due to the larger size and lateral structure of the motor cortex. Future investigation focused on spatial resolution of sub-scalp electrodes would provide further insight.

*4.2.2. Classification* Using linear discriminant analysis we discriminated motor-related neural activity significantly above chance. This alone would allow for simple binary outputs that are useful for certain BCI applications in persons with severe disability, such as alerting carers, clicking in digital environments that use an automated scroll, and binary communication protocols. Chronic sub-scalp EEG implantation can provide the opportunity to collect large datasets that allow for training of feature selection and machine learning algorithms with more parameters that may produce better performance and increased dimensional control for users. Previous studies have demonstrated two- [24, 25] and three-dimensional control [26] using non-invasive EEG. We expect sub-scalp EEG BCI performance to at least match non-invasive counterparts with equivalent channel setups due to improved stability, and increased amplitude from avoiding attenuation through scalp tissue.

Demonstrating classification of motor cortex activity, despite the various challenges associated with the data collection for this experiment, support the use of sub-scalp BCI for in-home, everyday use. During data recording, the sheep were in noisy environments: surrounded by distractions of other noisy sheep, impatient for food, chewing, and vocalising. There was no Faraday cage to remove external electrical interference. Additionally, while the animals did perform left and right head movements, these movements were often inconsistent, paired with upward or downward motion, slow or fast, and preceded by inactivity, eating, vocalising, stomping, or other motions. All of these factors contributed to EEG noise in this experiment and, despite these factors, we were able to discriminate motor activity. Unlike controlled laboratory or clinical environments, in-home BCI users will be

surrounded by other devices, people, and distractions, and will not utilise large, expensive, sophisticated amplification equipment. Reliable control is essential for user acceptance of BCI devices. This study has demonstrated sub-scalp EEG has the potential to provide reliability as a sensorimotor BCI outside of controlled laboratory environments.

In this experiment, sub-scalp EEG has demonstrated comparable performance with similar work investigating endovascular electrode arrays. Forsyth et al. [48] were able to decode left vs. right discrimination significantly above chance in 50% of sheep with endovascular data (maximum accuracy = 70%,  $n=2$ ), as were we with sub-scalp electrodes (test set accuracy = 66%,  $n=4$ ). Discrimination between grouped left and right movement and rest was achieved in both sheep with endovascular electrodes, reporting a maximum classification accuracy of 80% and 90% [48]. While we did not group both directions into a single class, similar performance was observed for rest class sensitivity ( $74\pm1\%$ ) and specificity ( $82\pm5\%$ ). The comparable signal quality between sub-scalp EEG in this study and endovascular electrodes as per Forsyth et al. [48] is consistent with previous work comparing these two recording modalities [33]. Since the work of Forsyth et al. [48], the endovascular BCI approach has progressed into human trials, demonstrating efficacy as a chronic, in-home system by providing benefit to persons with ALS [60].

While comparable motor decoding studies in sheep models are limited, substantial literature exists regarding motor decoding in humans across non-invasive EEG, ECoG, and endovascular modalities. ECoG arrays have consistently achieved high-accuracy decoding for a broad spectrum of motor activity, including hand and elbow postures [61], finger movement [62], and speech [27]. A direct comparison by Liao et al. [63] on pairwise finger movement decoding between non-invasive EEG and ECoG revealed average accuracies of 77% and 91%, respectively. Similarly, studies on speech decoding from non-invasive EEG have demonstrated high classification accuracy ( $>80\%$ ) for limited vocabularies (e.g., “left”, “down”, “right”, “up”, and “select”) [64, 65]. However, these have not yet achieved the accuracy levels comparable to ECoG speech decoding systems [66]. ECoG recordings provide a clear improvement in BCI functionality over non-invasive EEG. While signal quality of endovascular electrodes has been shown to be generally higher than non-invasive EEG [67] and comparable to ECoG [44], this fidelity has not yet translated to BCI functionality. Preliminary in-human endovascular BCI studies have reported classification accuracies of 91% and 70% (from two patients) for four gross hand

and foot motor execution classes [68], providing a benchmark for current minimally invasive BCI performance. However, as endovascular arrays evolve to access smaller, peripheral vasculature and record from broader neural populations, improved BCI performance is anticipated. Given the inherent challenges of replicating complex motor decoding experiments in animal models, future investigations should prioritise evaluating the performance of sub-scalp EEG as a BCI in human subjects, to determine if this modality can achieve comparable success to that demonstrated here in sheep models.

#### *4.3. Feasibility of Sub-scalp BCI*

Overall, we have completed both aims of this study and provide evidence in support of sub-scalp EEG for BCI applications. BCIs have demonstrated functionality across diverse signal acquisition modalities, including non-invasive EEG and invasive techniques like ECoG and endovascular electrodes. The spatial resolution of the signal acquisition methods significantly impacts the capabilities of the BCI system. High EEG spatial resolution means the recordings can be attributed to highly localised regions of the brain. Humans have demonstrated the ability to learn to modulate regions of the motor cortex when provided with feedback [26, 69, 70]. In the context of BCI applications, decoded modulations can provide input into any number of devices, allowing the user direct control of the device through their neural activity. High spatial resolution means the ability to decode from more localised regions of the cortex. If the user learns to modulate these localised regions independently, this leads to higher dimensional control that, in turn, results in improved BCI function and user acceptance.

While spatial resolution of EEG is typically stated as in the order of centimetres [40–43], higher density, non-invasive arrays have been shown to provide high signal quality, and even identify underlying gyri and sulci [47]. High density arrays can isolate activity from local brain regions that may lead to high functioning BCIs [71]. However, as the number of electrodes increases, so too does the difficulty of setting up and maintaining non-invasive EEG systems. Incorporating high-density arrays into sub-scalp EEG systems results in no added setup or maintenance from the user’s perspective. In this way, sub-scalp EEG systems offer a continuous, long-term recording solution capable of signal quality equivalent to the highest resolution non-invasive EEG systems currently available, and with none of the daily setup.



ECoG and endovascular electrodes have demonstrated an optimal inter-channel distance between 1 and 10 mm in humans [40, 45] and sheep models [44]. The results of this study suggest that the optimal inter-channel distance for sub-scalp EEG recordings is 5 mm or less, indicating that sub-scalp EEG spatial resolution may be closer to intracranial than non-invasive electrodes. While these results are preliminary and subject to limitations, they offer evidence that sub-scalp EEG can record with high spatial resolution, and may allow for high performance BCIs without the need to enter the skull. ECoG BCI systems have demonstrated high bandwidth and utility by allowing users to communicate with BCI spellers, or control computers, prosthetics, and wheelchairs [72]. More recently, ECoG arrays has shown promise as part of BCIs for decoding non-verbal user’s speech [27, 73, 74]. These technologies may be of assistance to a broad range of cohorts with physical and verbal disability. However, the risk of sub-cranial implantation may deter these cohorts from accessing ECoG BCIs. Endovascular arrays mitigate this risk, however are still more invasive than sub-scalp arrays, and carry risk of stenosis and thrombosis [16–18]. We demonstrated comparable motor decoding performance between endovascular and sub-scalp arrays. Should sub-scalp BCI demonstrate comparable utility to ECoG BCIs, it has the potential for tremendous impact, providing significant improvement to quality of life by restoring fundamental abilities such as speech and mobility, across a broad range of users.

The major limitation of this work is the use of sheep models. Sheep models have significant anatomical differences to human models, including skull thickness, brain size, and sensory and motor cortex structure. While we have also included and compared with results from previous studies that have explored ECoG and endovascular spatial resolution in sheep models [44], future work should endeavour to determine sub-scalp EEG signal qualities and BCI performance in humans.

## **5. Conclusion**

Non-invasive recording of sensorimotor neural activity has demonstrated utility as input for BCI applications in previous studies. However, user acceptance of these systems for chronic BCI applications is low. Sub-scalp EEG is a minimally invasive alternative BCI signal acquisition method that addresses limitations of existing and emerging chronic technologies. We have demonstrated sub-scalp recording of sensorimotor rhythms in sheep models, identified important spatial, temporal, and

spectral features, and classified motor execution with above chance performance. Our results are comparable to previous work investigating SEP signal quality [44] and classification of motor-related neural activity [48] using ECoG and endovascular arrays in sheep models. These findings support further investigation into sub-scalp BCI technology as a tool for assisting persons with chronic physical disability with everyday activities. Future work should focus on characterising sub-scalp EEG spatial resolution, understanding the potential BCI user acceptance of sub-scalp technology, and in-human sub-scalp BCI clinical studies.

### Acknowledgments

We thank veterinary technician Tomas Vale and animal handler Quan Nguyen (The Florey Institute of Neuroscience and Mental Health) for their assistance in caring for the animals, surgical preparations, and monitoring during the animal experiments.

We also express our appreciation for the animals used for this research. Animal studies are crucial for the realisation of medical devices. We intend to ensure insights gained from their sacrifice lead to improved quality of life for persons with severe disability.

TB Mahoney was supported by the Australian Government Research Training Program Scholarship, Elizabeth and Vernon Puzey Scholarship, and the PhD Write-Up Award (Faculty of Engineering and Information Technology) from the University of Melbourne, Australia.

There are no conflicts of interest to report.

All raw data is available through the Figshare database for experiments pertaining to both Aim 1 [75] and Aim 2 [76].

### References

- [1] Marialuisa Zedde, Ilaria Grisendi, Francesca Romana Pezzella, Manuela Napoli, Claudio Moratti, Franco Valzania, and Rosario Pascarella. Acute Onset Quadriplegia and Stroke: Look at the Brainstem, Look at the Midline. *Journal of Clinical Medicine*, 11(23):7205, December 2022. ISSN 2077-0383. doi: 10.3390/jcm11237205. URL <https://www.mdpi.com/2077-0383/11/23/7205>.
- [2] Roman Haberl, Dennis G. Vollmer, and Werner Hacke. Tetraplegia and Paraplegia. In Werner Hacke, Daniel F. Hanley, Karl M. Einhäupl, Thomas P.

- Bleck, Michael N. Diring, and Allan H. Ropper, editors, *Neurocritical Care*, pages 292–306. Springer Berlin Heidelberg, Berlin, Heidelberg, 1994. ISBN 978-3-642-87604-2 978-3-642-87602-8. doi: 10.1007/978-3-642-87602-8\_28. URL [http://link.springer.com/10.1007/978-3-642-87602-8\\_28](http://link.springer.com/10.1007/978-3-642-87602-8_28).
- [3] Md Samiul Haque Sunny, Md Ishrak Islam Zarif, Ivan Rulik, Javier Sanjuan, Mohammad Habibur Rahman, Sheikh Iqbal Ahamed, Inga Wang, Katie Schultz, and Brahim Brahmi. Eye-gaze control of a wheelchair mounted 6DOF assistive robot for activities of daily living. *Journal of NeuroEngineering and Rehabilitation*, 18(1):173, December 2021. ISSN 1743-0003. doi: 10.1186/s12984-021-00969-2. URL <https://jneuroengrehab.biomedcentral.com/articles/10.1186/s12984-021-00969-2>.
- [4] Alexandre Bissoli, Daniel Lavino-Junior, Mariana Sime, Lucas Encarnação, and Teodiano Bastos-Filho. A Human–Machine Interface Based on Eye Tracking for Controlling and Monitoring a Smart Home Using the Internet of Things. *Sensors*, 19(4):859, February 2019. ISSN 1424-8220. doi: 10.3390/s19040859. URL <http://www.mdpi.com/1424-8220/19/4/859>.
- [5] A. Kübler, F. Nijboer, J. Mellinger, T. M. Vaughan, H. Pawelzik, G. Schalk, D. J. McFarland, N. Birbaumer, and J. R. Wolpaw. Patients with ALS can use sensorimotor rhythms to operate a brain-computer interface. *Neurology*, 64(10):1775–7, 2005. ISSN 0028-3878. doi: 10.1212/01.Wnl.0000158616.43002.6d. Type: Journal Article.
- [6] Han Yuan and Bin He. Brain–Computer Interfaces Using Sensorimotor Rhythms: Current State and Future Perspectives. *IEEE Transactions on Biomedical Engineering*, 61(5):1425–1435, May 2014. ISSN 0018-9294, 1558-2531. doi: 10.1109/TBME.2014.2312397. URL <http://ieeexplore.ieee.org/document/6775293/>.
- [7] Betts Peters, Gregory Bieker, Susan M. Heckman, Jane E. Huggins, Catherine Wolf, Debra Zeitlin, and Melanie Fried-Oken. Brain-Computer Interface Users Speak Up: The Virtual Users’ Forum at the 2013 International Brain-Computer Interface Meeting. *Archives of Physical Medicine and Rehabilitation*, 96(3, Supplement):S33–S37, 2015. ISSN 0003-9993. doi: 10.1016/j.apmr.2014.03.037. Type: Journal Article.
- [8] Christine H. Blabe, Vikash Gilja, Cindy A. Chestek, Krishna V. Shenoy, Kim D. Anderson, and Jaimie M. Henderson. Assessment of brain-machine interfaces

- from the perspective of people with paralysis. *Journal of Neural Engineering*, 12(4):043002, 2015. ISSN 1741-2560 1741-2552. doi: 10.1088/1741-2560/12/4/043002. Type: Journal Article.
- [9] A. Kubler, E. M. Holz, A. Riccio, C. Zickler, T. Kaufmann, S. C. Kleih, P. Staiger-Salzer, L. Desideri, E. J. Hoogerwerf, and D. Mattia. The user-centered design as novel perspective for evaluating the usability of BCI-controlled applications. *PLoS One*, 9(12):e112392, 2014. ISSN 1932-6203 (Electronic) 1932-6203 (Linking). doi: 10.1371/journal.pone.0112392. Type: Journal Article.
- [10] Ivo Käthner, Sebastian Halder, Christoph Hintermüller, Arnau Espinosa, Christoph Guger, Felip Miralles, Eloisa Vargiu, Stefan Dauwalder, Xavier Rafael-Palou, Marc Solà, Jean M. Daly, Elaine Armstrong, Suzanne Martin, and Andrea Kübler. A Multifunctional Brain-Computer Interface Intended for Home Use: An Evaluation with Healthy Participants and Potential End Users with Dry and Gel-Based Electrodes. *Frontiers in Neuroscience*, 11:286, May 2017. ISSN 1662-453X. doi: 10.3389/fnins.2017.00286. URL <http://journal.frontiersin.org/article/10.3389/fnins.2017.00286/full>.
- [11] Ana S. S. Cardoso, Lotte N. S. Andreasen Struijk, Rasmus L. Kaeseler, and Mads Jochumsen. Comparing the Usability of Alternative EEG Devices to Traditional Electrode Caps for SSVEP-BCI Controlled Assistive Robots. In *2022 International Conference on Rehabilitation Robotics (ICORR)*, pages 1–6, Rotterdam, Netherlands, July 2022. IEEE. ISBN 9781665488297. doi: 10.1109/ICORR55369.2022.9896588. URL <https://ieeexplore.ieee.org/document/9896588/>.
- [12] Jamie F M Brannigan, Kishan Liyanage, Hugo Layard Horsfall, Luke Bashford, William Muirhead, and Adam Fry. Brain-computer interfaces patient preferences: a systematic review. *Journal of Neural Engineering*, 21(6):061005, December 2024. ISSN 1741-2560, 1741-2552. doi: 10.1088/1741-2552/ad94a6. URL <https://iopscience.iop.org/article/10.1088/1741-2552/ad94a6>.
- [13] Thomas J Oxley, Peter E Yoo, Gil S Rind, Stephen M Ronayne, C M Sarah Lee, Christin Bird, Victoria Hampshire, Rahul P Sharma, Andrew Morokoff, Daryl L Williams, Christopher MacIsaac, Mark E Howard, Lou Irving, Ivan Vrljic, Cameron Williams, Sam E John, Frank Weissenborn, Madeleine Dzenko, Anna H Balabanski, David Friedenberg, Anthony N Burkitt, Yan T Wong,

- Katharine J Drummond, Patricia Desmond, Douglas Weber, Timothy Denison, Leigh R Hochberg, Susan Mathers, Terence J O'Brien, Clive N May, J Mocco, David B Grayden, Bruce C V Campbell, Peter Mitchell, and Nicholas L Opie. Motor neuroprosthesis implanted with neurointerventional surgery improves capacity for activities of daily living tasks in severe paralysis: first in-human experience. *Journal of NeuroInterventional Surgery*, 13(2):102–108, 2021. ISSN 1759-8478. doi: 10.1136/neurintsurg-2020-016862. URL <https://jniss.bmj.com/content/13/2/102>.
- [14] Jamie F.M. Brannigan, Adam Fry, Nicholas L. Opie, Bruce C.V. Campbell, Peter J. Mitchell, and Thomas J. Oxley. Endovascular Brain-Computer Interfaces in Poststroke Paralysis. *Stroke*, 55(2):474–483, February 2024. ISSN 0039-2499, 1524-4628. doi: 10.1161/STROKEAHA.123.037719. URL <https://www.ahajournals.org/doi/10.1161/STROKEAHA.123.037719>.
- [15] Anqi Zhang, Emiri T. Mandeville, Lijun Xu, Creed M. Stary, Eng H. Lo, and Charles M. Lieber. Ultraflexible endovascular probes for brain recording through micrometer-scale vasculature. *Science*, 381(6655):306–312, July 2023. ISSN 0036-8075, 1095-9203. doi: 10.1126/science.adh3916. URL <https://www.science.org/doi/10.1126/science.adh3916>.
- [16] Robert M. Starke, Tony Wang, Dale Ding, Christopher R. Durst, R. Webster Crowley, Nohra Chalouhi, David M. Hasan, Aaron S. Dumont, Pascal Jabbour, and Kenneth C. Liu. Endovascular Treatment of Venous Sinus Stenosis in Idiopathic Intracranial Hypertension: Complications, Neurological Outcomes, and Radiographic Results. *The Scientific World Journal*, 2015:140408, 2015. ISSN 2356-6140. doi: 10.1155/2015/140408. URL <https://doi.org/10.1155/2015/140408>. Type: Journal Article.
- [17] Kalgi Modi, Michael P. Soos, and Kunal Mahajan. Stent Thrombosis. In *StatPearls*. StatPearls Publishing, Treasure Island (FL), 2024. URL <http://www.ncbi.nlm.nih.gov/books/NBK441908/>.
- [18] Sauson Soldozy, Steven Young, Jeyan S. Kumar, Stepan Capek, Daniel R. Felbaum, Walter C. Jean, Min S. Park, and Hasan R. Syed. A systematic review of endovascular stent-electrode arrays, a minimally invasive approach to brain-machine interfaces. *Neurosurgical Focus*, 49(1):E3, July 2020. ISSN 1092-0684. doi: 10.3171/2020.4.FOCUS20186. URL <https://thejns.org/view/journals/neurosurg-focus/49/1/article-pE3.xml>.

- [19] Rachel E. Stirling, Matias I. Maturana, Philippa J. Karoly, Ewan S. Nurse, Kate McCutcheon, David B. Grayden, Steven G. Ringo, John M. Heasman, Rohan J. Hoare, Alan Lai, Wendyl D’Souza, Udaya Seneviratne, Linda Seiderer, Karen J. McLean, Kristian J. Bulluss, Michael Murphy, Benjamin H. Brinkmann, Mark P. Richardson, Dean R. Freestone, and Mark J. Cook. Seizure Forecasting Using a Novel Sub-Scalp Ultra-Long Term EEG Monitoring System. *Frontiers in Neurology*, 12(1445), 2021. ISSN 1664-2295. doi: 10.3389/fneur.2021.713794. Type: Journal Article.
- [20] Jonas Duun-Henriksen, Maxime Baud, Mark P. Richardson, Mark Cook, George Kouvas, John M. Heasman, Daniel Friedman, Jukka Peltola, Ivan C. Zibrandtsen, and Troels W. Kjaer. A new era in electroencephalographic monitoring? Subscalp devices for ultra-long-term recordings. *EPILEPSIA*, 2020. ISSN 00139580. doi: 10.1111/epi.16630. Type: Journal Article.
- [21] Sigge Weisdorf, Jonas Duun-Henriksen, Marianne J. Kjeldsen, Frantz R. Poulsen, Sirin W. Gangstad, and Troels W. Kjaer. Ultra-long-term subcutaneous home monitoring of epilepsy—490 days of EEG from nine patients. *Epilepsia*, 60(11):2204–2214, 2019. ISSN 0013-9580. doi: 10.1111/epi.16360. Type: Journal Article.
- [22] Sabry L. Barlatey, George Kouvas, Aleksander Sobolewski, Andreas Nowacki, Claudio Pollo, and Maxime O. Baud. Designing next-generation subscalp devices for seizure monitoring: A systematic review and meta-analysis of established extracranial hardware. *Epilepsy Research*, 202:107356, May 2024. ISSN 09201211. doi: 10.1016/j.eplepsyres.2024.107356. URL <https://linkinghub.elsevier.com/retrieve/pii/S0920121124000718>.
- [23] Zulfi Haneef, Kaiyuan Yang, Sameer A. Sheth, Fuad Z. Aloor, Behnaam Aazhang, Vaishnav Krishnan, and Cemal Karakas. Sub-scalp electroencephalography: A next-generation technique to study human neurophysiology. *Clinical Neurophysiology*, 141:77–87, 2022. ISSN 1388-2457. doi: 10.1016/j.clinph.2022.07.003. URL <https://www.sciencedirect.com/science/article/pii/S1388245722003273>.
- [24] Dandan Huang, P. Lin, Ding-Yu Fei, Xuedong Chen, and Ou Bai. EEG-based online two-dimensional cursor control. In *2009 Annual International Conference of the IEEE Engineering in Medicine and Biology Society*, pages 4547–4550,

- Minneapolis, MN, September 2009. IEEE. doi: 10.1109/IEMBS.2009.5332722. URL <http://ieeexplore.ieee.org/document/5332722/>.
- [25] Turan A Kayagil, Ou Bai, Craig S Henriquez, Peter Lin, Stephen J Furlani, Sherry Vorbach, and Mark Hallett. A binary method for simple and accurate two-dimensional cursor control from EEG with minimal subject training. *Journal of NeuroEngineering and Rehabilitation*, 6(1):14, December 2009. ISSN 1743-0003. doi: 10.1186/1743-0003-6-14. URL <https://jneuroengrehab.biomedcentral.com/articles/10.1186/1743-0003-6-14>.
- [26] Dennis J McFarland, William A Sarnacki, and Jonathan R Wolpaw. Electroencephalographic (EEG) control of three-dimensional movement. *Journal of Neural Engineering*, 7(3):036007, June 2010. ISSN 1741-2560, 1741-2552. doi: 10.1088/1741-2560/7/3/036007. URL <https://iopscience.iop.org/article/10.1088/1741-2560/7/3/036007>.
- [27] Kaylo T. Littlejohn, Cheol Jun Cho, Jessie R. Liu, Alexander B. Silva, Bohan Yu, Vanessa R. Anderson, Cady M. Kurtz-Miott, Samantha Brosler, Anshul P. Kashyap, Irina P. Hallinan, Adit Shah, Adelyn Tu-Chan, Karunesh Ganguly, David A. Moses, Edward F. Chang, and Gopala K. Anumanchipalli. A streaming brain-to-voice neuroprosthesis to restore naturalistic communication. *Nature Neuroscience*, 28(4):902–912, April 2025. ISSN 1097-6256, 1546-1726. doi: 10.1038/s41593-025-01905-6. URL <https://www.nature.com/articles/s41593-025-01905-6>.
- [28] Paul L. Nunez and Ramesh Srinivasan. *Electric Fields of the Brain*. Oxford University Press, January 2006. ISBN 978-0-19-505038-7. doi: 10.1093/acprof:oso/9780195050387.001.0001. URL <http://www.oxfordscholarship.com/view/10.1093/acprof:oso/9780195050387.001.0001/acprof-9780195050387>.
- [29] G. Bryan Young, John R. Ives, Martin G. Chapman, and Seyed M. Mirsattari. A comparison of subdermal wire electrodes with collodion-applied disk electrodes in long-term EEG recordings in ICU. *Clinical Neurophysiology*, 117(6):1376–1379, 2006. ISSN 1388-2457. doi: 10.1016/j.clinph.2006.02.006. Type: Journal Article.
- [30] Jonas Duun-Henriksen, Troels Wesenberg Kjaer, David Looney, Mary Doreen Atkins, Jens Ahm Sørensen, Martin Rose, Danilo P. Mandic, Rasmus Elsborg Madsen, and Claus Bogh Juhl. EEG Signal Quality of a Subcutaneous Recording System Compared to Standard Surface Electrodes. *Journal of Sensors*, 2015:

- 341208, 2015. ISSN 1687-725X. doi: 10.1155/2015/341208. Type: Journal Article.
- [31] Sigge Weisdorf, Sirin W. Gangstad, Jonas Duun-Henriksen, Karina S. S. Mosholt, and Troels W. Kjær. High similarity between EEG from subcutaneous and proximate scalp electrodes in patients with temporal lobe epilepsy. *Journal of Neurophysiology*, 120(3):1451–1460, 2018. ISSN 0022-3077. doi: 10.1152/jn.00320.2018. Type: Journal Article.
- [32] Jared D. Olson, Jeremiah D. Wander, Lise Johnson, Devapratim Sarma, Kurt Weaver, Edward J. Novotny, Jeffrey G. Ojemann, and Felix Darvas. Comparison of subdural and subgaleal recordings of cortical high-gamma activity in humans. *Clinical neurophysiology : official journal of the International Federation of Clinical Neurophysiology*, 127(1):277–284, 2016. ISSN 1872-8952 1388-2457. doi: 10.1016/j.clinph.2015.03.014. Type: Journal Article.
- [33] Timothy B. Mahoney, Po-Chen Liu, David B. Grayden, and Sam E. John. Comparison of Sub-Scalp EEG and Endovascular Stent-Electrode Array for Visual Evoked Potential Brain-Computer Interface. In *2023 45th Annual International Conference of the IEEE Engineering in Medicine & Biology Society (EMBC)*, pages 1–4, Sydney, Australia, July 2023. IEEE. ISBN 9798350324471. doi: 10.1109/EMBC40787.2023.10340834. URL <https://ieeexplore.ieee.org/document/10340834/>.
- [34] K. Yang, L. Tong, J. Shu, N. Zhuang, B. Yan, and Y. Zeng. High Gamma Band EEG Closely Related to Emotion: Evidence From Functional Network. *Front Hum Neurosci*, 14:89, 2020. ISSN 1662-5161 (Print) 1662-5161. doi: 10.3389/fnhum.2020.00089. Type: Journal Article.
- [35] Matthew S. Fifer, Guy Hotson, Brock A. Wester, David P. McMullen, Yujing Wang, Matthew S. Johannes, Kapil D. Katyal, John B. Helder, Matthew P. Para, R. Jacob Vogelstein, William S. Anderson, Nitish V. Thakor, and Nathan E. Crone. Simultaneous Neural Control of Simple Reaching and Grasping With the Modular Prosthetic Limb Using Intracranial EEG. *IEEE Transactions on Neural Systems and Rehabilitation Engineering*, 22(3):695–705, 2014. doi: 10.1109/TNSRE.2013.2286955.
- [36] Paul J. Fitzgerald and Brendon O. Watson. Gamma oscillations as a biomarker for major depression: an emerging topic. *Translational Psychiatry*, 8(1):177,



- September 2018. ISSN 2158-3188. doi: 10.1038/s41398-018-0239-y. URL <https://doi.org/10.1038/s41398-018-0239-y>.
- [37] Peter Trautner, Timm Rosburg, Thomas Dietl, Jürgen Fell, OA Korzyukov, Martin Kurthen, Carlo Schaller, Christian Erich Elger, and Nash N Boutros. Sensory gating of auditory evoked and induced gamma band activity in intracranial recordings. *Neuroimage*, 32(2):790–798, 2006. doi: 10.1016/j.neuroimage.2006.04.203. Publisher: Elsevier.
- [38] Jean-Philippe Lachaux, Nathalie George, Catherine Tallon-Baudry, Jacques Martinerie, Laurent Hugueville, Lorella Minotti, Philippe Kahane, and Bernard Renault. The many faces of the gamma band response to complex visual stimuli. *NeuroImage*, 25(2):491–501, 2005. ISSN 1053-8119. doi: 10.1016/j.neuroimage.2004.11.052. URL <https://www.sciencedirect.com/science/article/pii/S1053811904007347>.
- [39] Nelly Mainy, Julien Jung, Monica Baciú, Philippe Kahane, Benjamin Schoendorff, Lorella Minotti, Dominique Hoffmann, Olivier Bertrand, and Jean-Philippe Lachaux. Cortical dynamics of word recognition. *Human brain mapping*, 29(11):1215–1230, 2008. doi: 10.1002/hbm.20457. Publisher: Wiley Online Library.
- [40] Marc W Slutzky, Luke R Jordan, Todd Krieg, Ming Chen, David J Mogul, and Lee E Miller. Optimal spacing of surface electrode arrays for brain-machine interface applications. *Journal of Neural Engineering*, 7(2):026004, April 2010. ISSN 1741-2560, 1741-2552. doi: 10.1088/1741-2560/7/2/026004. URL <https://iopscience.iop.org/article/10.1088/1741-2560/7/2/026004>.
- [41] A. Robert Spitzer, Leonardo G. Cohen, Judy Fabrikant, and Mark Hallett. A method for determining optimal interelectrode spacing for cerebral topographic mapping. *Electroencephalography and Clinical Neurophysiology*, 72(4):355–361, April 1989. ISSN 00134694. doi: 10.1016/0013-4694(89)90072-2. URL <https://linkinghub.elsevier.com/retrieve/pii/0013469489900722>.
- [42] R. Srinivasan, P.L. Nunez, and R.B. Silberstein. Spatial filtering and neocortical dynamics: estimates of EEG coherence. *IEEE Transactions on Biomedical Engineering*, 45(7):814–826, July 1998. ISSN 00189294. doi: 10.1109/10.686789. URL <http://ieeexplore.ieee.org/document/686789/>.
- [43] Walter J. Freeman, Mark D. Holmes, Brian C. Burke, and Sampsa Vanhatalo. Spatial spectra of scalp EEG and EMG from awake humans. *Clinical*

- Neurophysiology*, 114(6):1053–1068, June 2003. ISSN 13882457. doi: 10.1016/S1388-2457(03)00045-2. URL <https://linkinghub.elsevier.com/retrieve/pii/S1388245703000452>.
- [44] Sam E. John, Nicholas L. Opie, Yan T. Wong, Gil S. Rind, Stephen M. Ronayne, Giulia Gerboni, Sebastien H. Bauquier, Terence J. O’Brien, Clive N. May, David B. Grayden, and Thomas J. Oxley. Signal quality of simultaneously recorded endovascular, subdural and epidural signals are comparable. *Scientific Reports*, 8(1):8427, 2018. ISSN 2045-2322. doi: 10.1038/s41598-018-26457-7. URL <https://doi.org/10.1038/s41598-018-26457-7>. Type: Journal Article.
- [45] Walter J Freeman, Linda J Rogers, Mark D Holmes, and Daniel L Silbergeld. Spatial spectral analysis of human electrocorticograms including the alpha and gamma bands. *Journal of Neuroscience Methods*, 95(2):111–121, February 2000. ISSN 01650270. doi: 10.1016/S0165-0270(99)00160-0. URL <https://linkinghub.elsevier.com/retrieve/pii/S0165027099001600>.
- [46] M. R. Nuwer. Localization of Motor Cortex with Median Nerve Somatosensory Evoked Potentials. In Johannes Schramm and Aage R. Møller, editors, *Intraoperative Neurophysiologic Monitoring in Neurosurgery*, pages 63–71. Springer Berlin Heidelberg, Berlin, Heidelberg, 1991. ISBN 9783642757525 9783642757501. doi: 10.1007/978-3-642-75750-1\_8. URL [http://link.springer.com/10.1007/978-3-642-75750-1\\_8](http://link.springer.com/10.1007/978-3-642-75750-1_8).
- [47] Leonhard Schreiner, Michael Jordan, Sebastian Sieghartsleitner, Christoph Kapeller, Harald Pretl, Kyousuke Kamada, Priscella Asman, Nuri F. Ince, Kai J. Miller, and Christoph Guger. Mapping of the central sulcus using non-invasive ultra-high-density brain recordings. *Scientific Reports*, 14(1): 6527, March 2024. ISSN 2045-2322. doi: 10.1038/s41598-024-57167-y. URL <https://www.nature.com/articles/s41598-024-57167-y>.
- [48] Ian A. Forsyth, Megan Dunston, Gabriel Lombardi, Gil S. Rind, Stephen Ronayne, Yan T. Wong, Clive N May, David B. Grayden, Thomas Oxley, Nicholas Opie, and Sam E. John. Evaluation of a minimally invasive endovascular neural interface for decoding motor activity. In *2019 9th International IEEE/EMBS Conference on Neural Engineering (NER)*, pages 750–753, 2019. doi: 10.1109/NER.2019.8717000.
- [49] Sam E. John, Timothy J.H. Lovell, Nicholas L. Opie, Stefan Wilson,

- Theodore C. Scordas, Yan T. Wong, Gil S. Rind, Stephen Ronayne, Sébastien H. Bauquier, Clive N. May, David B. Grayden, Terence J. O'Brien, and Thomas J. Oxley. The ovine motor cortex: A review of functional mapping and cytoarchitecture. *Neuroscience & Biobehavioral Reviews*, 80:306–315, September 2017. ISSN 01497634. doi: 10.1016/j.neubiorev.2017.06.002. URL <https://linkinghub.elsevier.com/retrieve/pii/S0149763417300726>.
- [50] Jonathan Wolpaw and Elizabeth Winter Wolpaw. *Brain–Computer Interfaces: Principles and Practice*. Oxford University Press, January 2012. ISBN 978-0-19-538885-5. doi: 10.1093/acprof:oso/9780195388855.001.0001. URL <http://www.oxfordscholarship.com/view/10.1093/acprof:oso/9780195388855.001.0001/acprof-9780195388855>.
- [51] Nicholas L. Opie, Sam E. John, Gil S. Rind, Stephen M. Ronayne, Yan T. Wong, Giulia Gerboni, Peter E. Yoo, Timothy J. H. Lovell, Theodore C. M. Scordas, Stefan L. Wilson, Anthony Dornom, Thomas Vale, Terence J. O'Brien, David B. Grayden, Clive N. May, and Thomas J. Oxley. Focal stimulation of the sheep motor cortex with a chronically implanted minimally invasive electrode array mounted on an endovascular stent. *Nature Biomedical Engineering*, 2(12):907–914, December 2018. ISSN 2157-846X. doi: 10.1038/s41551-018-0321-z. URL <https://www.nature.com/articles/s41551-018-0321-z>.
- [52] Thomas J. Oxley, Nicholas L. Opie, Sam E. John, Gil S. Rind, Stephen M. Ronayne, Tracey L. Wheeler, Jack W. Judy, Alan J. McDonald, Anthony Dornom, Timothy J. H. Lovell, Christopher Steward, David J. Garrett, Bradford A. Moffat, Elaine H. Lui, Nawaf Yassi, Bruce C. V. Campbell, Yan T. Wong, Kate E. Fox, Ewan S. Nurse, Iwan E. Bennett, Sébastien H. Bauquier, Kishan A. Liyanage, Nicole R. van der Nagel, Piero Perucca, Arman Ahnood, Katherine P. Gill, Bernard Yan, Leonid Churilov, Christopher R. French, Patricia M. Desmond, Malcolm K. Horne, Lynette Kiers, Steven Prawer, Stephen M. Davis, Anthony N. Burkitt, Peter J. Mitchell, David B. Grayden, Clive N. May, and Terence J. O'Brien. Minimally invasive endovascular stent-electrode array for high-fidelity, chronic recordings of cortical neural activity. *Nature Biotechnology*, 34(3):320–327, 2016. ISSN 1546-1696. doi: 10.1038/nbt.3428. URL <https://doi.org/10.1038/nbt.3428>. Type: Journal Article.
- [53] Brian C. Ross. Mutual Information between Discrete and Continuous Data Sets.

- PLoS ONE*, 9(2):e87357, February 2014. ISSN 1932-6203. doi: 10.1371/journal.pone.0087357. URL <https://dx.plos.org/10.1371/journal.pone.0087357>.
- [54] John O’Toole, M. Mutual Information, 2020. URL [https://github.com/otoolej/mutual\\_info\\_kNN](https://github.com/otoolej/mutual_info_kNN).
- [55] G Gerboni, S E John, G S Rind, S M Ronayne, C N May, T J Oxley, D B Grayden, N L Opie, and Y T Wong. Visual evoked potentials determine chronic signal quality in a stent-electrode endovascular neural interface. *Biomedical Physics & Engineering Express*, 4(5):055018, August 2018. ISSN 2057-1976. doi: 10.1088/2057-1976/aad714. URL <https://iopscience.iop.org/article/10.1088/2057-1976/aad714>.
- [56] Ravi Vakani and Dileep R. Nair. Electrocorcography and functional mapping. In *Handbook of Clinical Neurology*, volume 160, pages 313–327. Elsevier, 2019. ISBN 9780444640321. doi: 10.1016/B978-0-444-64032-1.00020-5. URL <https://linkinghub.elsevier.com/retrieve/pii/B9780444640321000205>.
- [57] Gerwin Schalk and Eric C. Leuthardt. Brain-Computer Interfaces Using Electrocorcographic Signals. *IEEE Reviews in Biomedical Engineering*, 4:140–154, 2011. ISSN 1937-3333, 1941-1189. doi: 10.1109/RBME.2011.2172408. URL <http://ieeexplore.ieee.org/document/6047564/>.
- [58] Jonathan Wolpaw and Elizabeth Winter Wolpaw. *Brain-Computer Interfaces: Principles and Practice, Chapter 7*. Oxford University Press, January 2012. ISBN 978-0-19-538885-5. doi: 10.1093/acprof:oso/9780195388855.001.0001. URL <http://www.oxfordscholarship.com/view/10.1093/acprof:oso/9780195388855.001.0001/acprof-9780195388855>.
- [59] G. Pfurtscheller. Chapter 26 Spatiotemporal ERD/ERS patterns during voluntary movement and motor imagery. In *Supplements to Clinical Neurophysiology*, volume 53, pages 196–198. Elsevier, 2000. ISBN 978-0-444-50499-9. doi: 10.1016/S1567-424X(09)70157-6. URL <https://linkinghub.elsevier.com/retrieve/pii/S1567424X09701576>.
- [60] Peter Mitchell, Sarah C. M. Lee, Peter E. Yoo, Andrew Morokoff, Rahul P. Sharma, Daryl L. Williams, Christopher MacIsaac, Mark E. Howard, Lou Irving, Ivan Vrljic, Cameron Williams, Steven Bush, Anna H. Balabanski, Katharine J. Drummond, Patricia Desmond, Douglas Weber, Timothy Denison, Susan Mathers, Terence J. O’Brien, J. Mocco, David B. Grayden, David S. Liebeskind, Nicholas L. Opie, Thomas J. Oxley, and Bruce C. V. Campbell.

- Assessment of Safety of a Fully Implanted Endovascular Brain-Computer Interface for Severe Paralysis in 4 Patients: The Stentrode With Thought-Controlled Digital Switch (SWITCH) Study. *JAMA Neurology*, 80(3):270–278, March 2023. ISSN 2168-6149. doi: 10.1001/jamaneurol.2022.4847. URL <https://doi.org/10.1001/jamaneurol.2022.4847>.
- [61] Takufumi Yanagisawa, Masayuki Hirata, Youichi Saitoh, Haruhiko Kishima, Kojiro Matsushita, Tetsu Goto, Ryohei Fukuma, Hiroshi Yokoi, Yukiyasu Kamitani, and Toshiki Yoshimine. Electrographic control of a prosthetic arm in paralyzed patients. *Annals of Neurology*, 71(3):353–361, March 2012. ISSN 0364-5134, 1531-8249. doi: 10.1002/ana.22613. URL <https://onlinelibrary.wiley.com/doi/10.1002/ana.22613>.
- [62] Lin Yao, Bingzhao Zhu, and Mahsa Shoaran. Fast and accurate decoding of finger movements from ECoG through Riemannian features and modern machine learning techniques. *Journal of Neural Engineering*, 19(1):016037, February 2022. ISSN 1741-2560, 1741-2552. doi: 10.1088/1741-2552/ac4ed1. URL <https://iopscience.iop.org/article/10.1088/1741-2552/ac4ed1>.
- [63] Ke Liao, Ran Xiao, Jania Gonzalez, and Lei Ding. Decoding Individual Finger Movements from One Hand Using Human EEG Signals. *PLoS ONE*, 9(1):e85192, January 2014. ISSN 1932-6203. doi: 10.1371/journal.pone.0085192. URL <https://dx.plos.org/10.1371/journal.pone.0085192>.
- [64] Luis Alfredo Moctezuma, Alejandro A. Torres-García, Luis Villaseñor-Pineda, and Maya Carrillo. Subjects identification using EEG-recorded imagined speech. *Expert Systems with Applications*, 118:201–208, March 2019. ISSN 09574174. doi: 10.1016/j.eswa.2018.10.004. URL <https://linkinghub.elsevier.com/retrieve/pii/S0957417418306468>.
- [65] Luis Alfredo Moctezuma and Marta Molinas. EEG-Based Subjects Identification Based on Biometrics of Imagined Speech Using EMD. In Shouyi Wang, Vicky Yamamoto, Jianzhong Su, Yang Yang, Erick Jones, Leon Iasemidis, and Tom Mitchell, editors, *Brain Informatics*, volume 11309, pages 458–467. Springer International Publishing, Cham, 2018. ISBN 9783030055868 9783030055875. doi: 10.1007/978-3-030-05587-5\_43. URL [http://link.springer.com/10.1007/978-3-030-05587-5\\_43](http://link.springer.com/10.1007/978-3-030-05587-5_43).
- [66] Diego Lopez-Bernal, David Balderas, Pedro Ponce, and Arturo Molina. A State-of-the-Art Review of EEG-Based Imagined Speech Decoding. *Frontiers*

- in *Human Neuroscience*, 16:867281, April 2022. ISSN 1662-5161. doi: 10.3389/fnhum.2022.867281. URL <https://www.frontiersin.org/articles/10.3389/fnhum.2022.867281/full>.
- [67] Brianna Thielen, Huijing Xu, Tatsuhiko Fujii, Shivani D Rangwala, Wenxuan Jiang, Michelle Lin, Alexandra Kammen, Charles Liu, Pradeep Selvan, Dong Song, William J Mack, and Ellis Meng. Making a case for endovascular approaches for neural recording and stimulation. *Journal of Neural Engineering*, 20(1):011001, February 2023. ISSN 1741-2560, 1741-2552. doi: 10.1088/1741-2552/acb086. URL <https://iopscience.iop.org/article/10.1088/1741-2552/acb086>.
- [68] Kriti Kacker, Nikole Chetty, Ariel K Feldman, James Bennett, Peter E Yoo, Adam Fry, David Lacomis, Noam Y Harel, Raul G Nogueira, Shahram Majidi, Nicholas L Opie, Jennifer L Collinger, Thomas J Oxley, David F Putrino, and Douglas J Weber. Motor activity in gamma and high gamma bands recorded with a Stentrode from the human motor cortex in two people with ALS. *Journal of Neural Engineering*, 22(2):026036, April 2025. ISSN 1741-2560, 1741-2552. doi: 10.1088/1741-2552/adbd78. URL <https://iopscience.iop.org/article/10.1088/1741-2552/adbd78>.
- [69] Jonathan R. Wolpaw and Dennis J. McFarland. Control of a two-dimensional movement signal by a noninvasive brain-computer interface in humans. *Proceedings of the National Academy of Sciences*, 101(51):17849–17854, December 2004. ISSN 0027-8424, 1091-6490. doi: 10.1073/pnas.0403504101. URL <https://pnas.org/doi/full/10.1073/pnas.0403504101>.
- [70] D. J. McFarland and J. R. Wolpaw. EEG-based brain-computer interfaces. *Current Opinion in Biomedical Engineering*, 4:194–200, 2017. ISSN 2468-4511. doi: 10.1016/j.cobme.2017.11.004. Type: Journal Article.
- [71] Hyemin S. Lee, Leonhard Schreiner, Seong-Hyeon Jo, Sebastian Sieghartsleitner, Michael Jordan, Harald Pretl, Christoph Guger, and Hyung-Soon Park. Individual finger movement decoding using a novel ultra-high-density electroencephalography-based brain-computer interface system. *Frontiers in Neuroscience*, 16:1009878, October 2022. ISSN 1662-453X. doi: 10.3389/fnins.2022.1009878. URL <https://www.frontiersin.org/articles/10.3389/fnins.2022.1009878/full>.
- [72] Kai J. Miller, Dora Hermes, and Nathan P. Staff. The current

- state of electrocorticography-based brain-computer interfaces. *Neurosurgical Focus*, 49(1):E2, July 2020. ISSN 1092-0684. doi: 10.3171/2020.4.FOCUS20185. URL <https://thejns.org/view/journals/neurosurg-focus/49/1/article-pE2.xml>.
- [73] Sean L. Metzger, Jessie R. Liu, David A. Moses, Maximilian E. Dougherty, Margaret P. Seaton, Kaylo T. Littlejohn, Josh Chartier, Gopala K. Anumanchipalli, Adelyn Tu-Chan, Karunesh Ganguly, and Edward F. Chang. Generalizable spelling using a speech neuroprosthesis in an individual with severe limb and vocal paralysis. *Nature Communications*, 13(1):6510, November 2022. ISSN 2041-1723. doi: 10.1038/s41467-022-33611-3. URL <https://www.nature.com/articles/s41467-022-33611-3>.
- [74] Alexander B. Silva, Kaylo T. Littlejohn, Jessie R. Liu, David A. Moses, and Edward F. Chang. The speech neuroprosthesis. *Nature Reviews Neuroscience*, 25(7):473–492, July 2024. ISSN 1471-003X, 1471-0048. doi: 10.1038/s41583-024-00819-9. URL <https://www.nature.com/articles/s41583-024-00819-9>.
- [75] Timothy Mahoney. SEP Stimulus Data, 2025. URL [https://figshare.unimelb.edu.au/articles/dataset/SEP\\_Stimulus\\_Data/28836644/1](https://figshare.unimelb.edu.au/articles/dataset/SEP_Stimulus_Data/28836644/1).
- [76] Timothy Mahoney. Behavioural Dataset, 2025. URL [https://figshare.unimelb.edu.au/articles/dataset/Behavioural\\_Dataset/28836473/1](https://figshare.unimelb.edu.au/articles/dataset/Behavioural_Dataset/28836473/1).